COHERENT FEEDBACK CONTROL AND NONLINEAR OPTICS IN CAVITY QED SYSTEMS

A DISSERTATION
SUBMITTED TO THE DEPARTMENT OF APPLIED PHYSICS
AND THE COMMITTEE ON GRADUATE STUDIES
OF STANFORD UNIVERSITY
IN PARTIAL FULFILLMENT OF THE REQUIREMENTS
FOR THE DEGREE OF
DOCTOR OF PHILOSOPHY

Hardeep Singh Sanghera

December 2016

This dissertation is online at: http://purl.stanford.edu/xc623vf0261

I certify that I have read this dissertation and that, in my opinion, it is fully adequate in scope and quality as a dissertation for the degree of Doctor of Philosophy.

Hideo Mabuchi, Primary Adviser

I certify that I have read this dissertation and that, in my opinion, it is fully adequate in scope and quality as a dissertation for the degree of Doctor of Philosophy.

Philip Bucksbaum

I certify that I have read this dissertation and that, in my opinion, it is fully adequate in scope and quality as a dissertation for the degree of Doctor of Philosophy.

Monika Schleier-Smith

Approved for the Stanford University Committee on Graduate Studies.

Patricia J. Gumport, Vice Provost for Graduate Education

This signature page was generated electronically upon submission of this dissertation in electronic format. An original signed hard copy of the signature page is on file in University Archives.

Abstract

In order to capitalize on their promise of high-bandwidth, ultra-low power operation, future nanophotonic devices will have to contend with quantum and coherent effects inherent to the small-volume, few-photon limit. The theoretical development of general, systematic frameworks for describing quantum feedback networks enables us to leverage established optical technologies, from single and multi-atom cavity quantum electrodynamics to ultrafast multimode optics, as an essential test bed for establishing direct contact between coherent-feedback control theory and first generation nanophotonic circuits.

For interesting regimes for photonic logic, we want to work where switching energies become on the order of attojoules. Within atomic cavity QED systems, this regime occurs where the number of atoms within the typical cavity is on the order of 1-10. In this regime, each atom is a quantum emitter and must be treated with a full quantum model. As the atom number is increased, a mean field theory can be applied and the dynamics can be modeled using the optical Bloch equations. Full quantum modelling of systems with the atom number > 10 are not tractable computationally and a simpler semi-classical model does not fully capture the dynamics correctly. Thus we must investigate an intermediate regime where it may not be necessary to

keep track of all quantum degrees of freedom and treat them semi-classically. I will present experimental data showing the effects of coherent feedback on a test cavity QED system alongside switching dynamics and other non-linear behavior in a few atom regime. Studying experimental data to help formulate new models will greatly help in the push towards practical optical non-linear systems for ultra low power photonic logic.

Acknowledgements

First and foremost, I would like to thank my research Adviser, Hideo Mabuchi, for everything he has given me. I was a confused first year graduate student looking for labs and Hideo gave me an opportunity to rotate through his lab. Almost immediately I knew I was going to stick around and do my PhD research here. The culture of the MabuchiLab that Hideo instilled really went a long way in making this group feel more like a family than just work colleagues. He was patient with me, allowed me the autonomy of leading the research in ways I saw fit and for that, I thank you.

Most of the skills I learned throughout my PhD years can be attributed to the teachings of former MabuchiLab alum/staff scientist Michael Armen (Dr. Mikey). When starting off in the MabuchiLab, I had very limited optics skills but Mikey was patient and an excellent teacher. Taught me everything I know about optics and was my go-to person for anything electronics related. It was a pleasure having worked alongside you. It's safe to say that without his help and support at the beginning of my grad school career, I would not have been able to accomplish the things that I have. I will always be in debt to you. Thank you.

I have had the pleasure to be around some of the brightest and nicest people during my time in MabuchiLab. There has been significant change to the group throughout my time here at Stanford but I can say that everyone has shown me the same friendship and support that comes with the MabuchiLab culture. I can seriously say that without my lab mates I would not be standing where I am today. My thesis work was only possible due to their help and support. A special thank you to Nikolas Tezak. He was my go to person whenever I needed any help with simulation and theory. I owe you big time buddy.

I also have to acknowledge my time at the University of British Columbia for my undergraduate degree. Before I could have even dreamt about coming to a prestigious school such as Stanford for a PhD, I had to learn the necessary life and academic skills through the undergraduate experience. All my professors had a significant role in providing me the knowledge and skills needed as a scientist and for that, I thank you. My original plan during undergrad was not to continue my education onto graduate school but to work as an engineer after the completion of my bachelors degree. However, the excellent curriculum of the Engineering Physics (Fizz) program at UBC opened up a lot of opportunities and exposed me also to the fundamental side of science rather than just the applied. Having a strong foundation in fundamental physics principles compounded with an electrical engineering program allowed me to become well-rounded and ready to take on anything. All this would not have been possible without the hard work and dedication of Fizz program director Dr. Andre Marziali. Just as importantly, I would like to thank Dr. Jon Nakane for giving us very unique opportunities to study science and engineering through hands on project lab work. Lastly, I certainly would not have gotten where I

am today without the friendship and support of my entire Fizz family. It was a rough journey but we still to this day can hold our heads up high for coming out in one piece.

Outside of my academic circles, I met a lot of great people during my time here at Stanford. I was given the opportunity to be part of the Stanford Bhangra family and I will cherish those friendships and memories forever. Even though I was usually one of few (or the only) grad students on the team and the large age gap between the rest of my teammates, it didn't take anything from experience and companionship I felt being around everyone. Bhangra gave me something to do for the times when I needed to take a break from grad school life. A special thank you to my friend and brother Jujhaar Singh who captained the team during my tenure. We learned a lot from each other, figuring out things together as we went along, and I can really say that I gained a true friend for life.

Last but certainly not least, I would like to give my family a big thank you. Family to me is above all and I would not be the person I am today without the unconditional love and support they have given me throughout my countless years in undergrad and grad school. To my mom and dad, I owe you guys everything. The sacrifices you guys made in coming to Canada from India and raising me and Parm while still working laborious jobs practically 7 days a week, we truly cannot thank you enough. I'm sorry if I have not been around or available as much as everyone would like. To my brother Parm: I know during my UBC times I was not around as much as I would've liked to help you as your older brother and I am sorry for that. But you have really shown me how smart and independent you have become and also taken on the responsibility of looking after and taking care of mom and

dad in my absence. Thank you. And to the rest of my Surrey family: all you guys had a part to play in my journey that allowed me to get to the spot I am today. Special thank you to Jyoti who has been with me almost since day 1 and made the trip out to support me at my dissertation defense. We can appreciate the grad student life and now that both of us are done, I am excited to see where life leads us next.

To my California family: Mamaji and Mamiji, you have treated me like your son and have become my parents away from home. My move from Canada to the Bay Area would not have worked as well as it did without your love and support. Everyone else, Sonu, Terry, Jeeta, Pardeep, and Gurvir, I may not say this much but it was your support and the caring environment you guys provided really is what helped me accomplish what I have in grad school. I knew I could count on you guys for anything and you would always be willing to help. Thank you.

Contents

List of Tables

List of Figures

Chapter 1

Introduction

1.1 Highlights from current computing technologies

This thesis explores a new way of approaching the topic of computing, a new paradigm which proposes the use of quantum mechanics in regards to devices and networks [1]. To see why this topic is of interest to us, we need to look back at how we got to the current level of computing technology and its future outlook. Current technologies which are used for classical computation are primarily based upon silicon semiconductor devices. The building block of this technology, the transistor, can be traced back to the work of John Bardeen, Walter Brattain, and William Shockley at Bell Labs in 1947 [2]. There has definitely been vast amounts of technological advances as it relates to the design and materials used for the transistor but the basic building block has remained fairly constant. We have been able to squeeze a lot out of this technology, as observed and stated by Intel co-founder Gordon Moore [3]. He noticed that since the 1960s, there has been an exponential growth in

silicon based computer chips with the number of transistors doubling approximately every two years. This observation came to be known as Moore's Law and has driven technological advancement to this day.

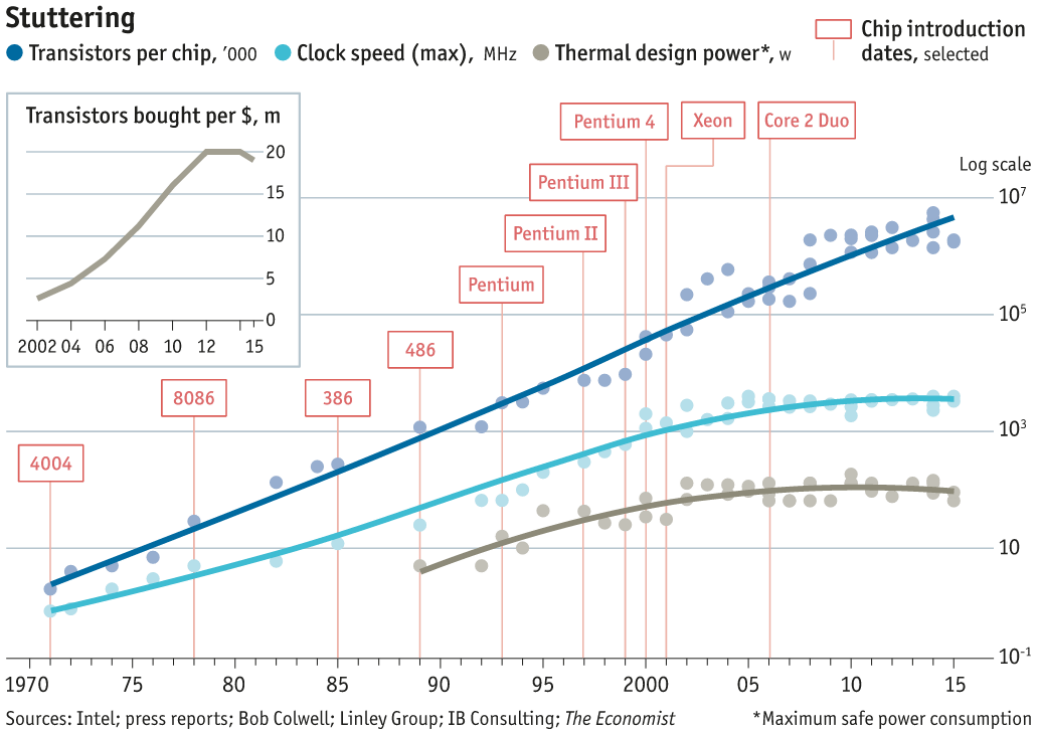

Figure 1.1: Moore's Law depicting exponential growth of silicon technology over the past four decades.

As shown in Figure 1.1, the trend predicted by Moore's law has lasted for over four decades [4]. However, we are at a crossroads. The current Silicon Roadmap, which outlines the advancements and guidelines for things such as feature size shrink, is set to end in 2020 [5]. With continual feature size reduction, we have approached a point where the distance scales of interest enter the regime of quantum mechanics. The roadmap has transistors with 5nm feature size set for 2020; at that feature size transistors will experience quantum tunnelling through their logic gates. This

poses quite the problem. How do we go about continuing these advancements of our computing technologies at an exponential rate? There is only so much we can do to play around with the design of silicon based transistors before we have squeezed all the possible computational potential out of the technology.

1.2 Looking towards a new approach

In order to continue on the exponential growth in computer technology that we have all grown accustomed to, we will have to shift away from the traditional paradigm and looks towards an approach completely different. Electronic devices have dominated this space, providing easy to design and manufacture devices but as previously discussed, are running into technical hurdles which will halt the progression of technology [6].

Photonic devices seem to be fitting for the void which electronic devices will leave. In applications where there are a vast amounts of interconnections between sub-components, nanophotonic architectures are very appealing with lower power, ultrafast operation. This approach is not entirely new. Photonic components are starting to be introduced into hybrid electronic/photonic circuits [7]. Optical interconnects between cores on a chip is hot research area. As of right now, a significant amount of energy is lost solely due to the distribution of a clock signal on an electronic chip and also the high bandwidth communication between individual cores in a multi-core processor. In this situation, photonic interconnections can provide a significant boost in performance without significant overhaul to the computing architecture.

Thinking more forward, what if we can replace the actual electronic building block which makes up today's computing technology? Photonic circuits give us access to regimes where interesting dynamics can be achieved at very low energy levels [8]. However, we quickly run into the hard fact that these devices are no longer *classical* devices but operate in a manner such that the quantum mechanical behavior of the internal workings becomes very important. Additionally, these quantum systems cannot be thought of the like the systems you study in undergraduate quantum mechanics. All those systems are closed as they can be represented by a wavefunction and evolution dictated by the internal Hamiltonian and the Schrödinger Equation. The quantum systems which come up in real life situations and the ones that are of interest to us are open quantum systems [9]. These systems are constantly interacting with the surrounding environment.

From a device perspective, individual photonic devices do not provide the robustness needed to make practical devices. Inherent quantum noise can be significant when operating at such low energy scales and thus behavior cannot be predicted. But we are not out of luck as this situation closely resembles the problem of control in classical engineering. You may have taken a class in control systems while studying engineering and know that systems put into the real world never act as you may predict. They are constantly being affected by outside influences which cannot be predicted beforehand. To overcome such issues, the idea of networks and feedback control exist. Such schemes are crucial to the design of systems and technologies that our modern society is built upon. Classical feedback control works by monitoring the state of the system of interest by measuring one or more of its

outputs and in turn applying feedback back to the system through actuators to control the system to some set point. The simplest example of feedback control that you may experience in your everyday life is your home thermostat. It works by measuring the temperature in the room and applies heating and cooling accordingly to keep the temperature at the set point.

Getting back to quantum devices, we can adopt the same concepts from classical control theory and apply them to quantum networks thus making new quantum devices which provide much more robust behavior in comparison to open loop systems. Measurement based feedback schemes, which classical controls systems are based upon, have been studied in quantum networks and have shown to provide effective results in control of such systems. However, as you may already suspect, performing a measurement on a quantum system disturbs the quantum state of the system, causing it to lose its quantum coherence, in turn introducing unwanted noise to the system [10]. Another more effective approach does exist, the idea of coherent feedback control. In such a scheme, the signals from a quantum system are coherently processed by another quantum system; you never convert the signal from the quantum system to an electrical signal, process it classically and feed it back. The entire feedback process is done passively. In such a scheme is where the true interest lies, allowing us to access the sought after low energy regimes.

At the heart of the photonic quantum devices of interest lies an optical nonlinearity [11]. The actual specifics of the optical system are not so strict. As long as you have an optical system which have been shown to exhibit some form of optical nonlinearity when interacting with an optical field, you can get interesting dynamics which in some

cases can be used for computing applications. Recent experiments with atomic cavity quantum electrodynamic (QED) systems [12][13][14][15], nitrogen vacancy centers [16], quantum dots, and intrinsic material nonlinearity have all shown to exhibit interesting behaviors which occur at very low energy scales. What they all show is that there is a very intriguing opportunity to exploit these dynamics for application in photonic signal processing. We will focus on a system where the nonlinearity comes from the dipole interaction of an alkali atom and cavity enhanced electric field. This type of system is the bread and butter of the MabuchiLab and we have extensive experience working with such setups.

1.3 Cavity nonlinear optics

The cavity QED system provides us with an excellent test bed to study various interesting low energy nonlinear optical behaviors [17]. With the microscopic sizes and electric field enhancement of the high finesse optical resonators, we are able to see interesting nonlinear dynamics in a system of a single atom and few photons. Previous experiments have explored regimes of both dispersive [18][19] and absorptive bistability [13][15][20], leading to dynamics which could be used a basis for classical information processing devices. When trying to explore the space of quantum networks, atomic quantum optical system provide us the best platform to try first principles experiments due to exhibiting extremely strong nonlinearities at ultra low probe energy scales. In addition, this space has been well studied [12] and we are able to perform experiments with parameters are the much more controllable in comparison to other nonlinear device platforms.

By utilizing the rich nonlinear dynamics observed in and individual cavity QED system, we will attempt to explore the role of coherent feedback as it pertains to giving us control over the system which we did not have before. In addition, by having the flexibility of a cavity QED system, we can explore dynamics over various energy regimes, looking at systems where the energy scales are more representative of practical devices, and also how to approach describing such interactions as they move away from feasible full quantum simulations but yet still cannot be fully captured by semiclassical models.

In Chapter 2 of this thesis, we will explore some of the theoretical background of cavity QED systems and also quantum networking. This will allow us to see the nonlinear dynamics that are possible at near single photon energy levels. Chapter 3 will give a broad overview of the experimental apparatus used to perform the experiments. Using this optical setup, we will discuss in Chapter 4 the measurements that were taken of this cavity QED system and the results from the experiments.

Chapter 2

Background

In this chapter we will introduce the quantum model for the cavity QED system. Building upon that we will discuss previous work done within the lab in regards to the canonical cavity QED system and results. Lastly we will introduce the idea of quantum networks and how we can go about modelling such systems. The system of interest for this thesis will be an example of how we can take simple cavity QED systems and build upon the results of previous work to manipulate them using networks and feedback to open up new dynamical regimes.

2.1 Cavity QED model

Our system of interest is actually quite simple and elegant. We have a two-level atom that is coupled to a cavity mode within an optical resonator and driven by a probe field. Figure 2.1 depicts a cartoon graphic of our system of interest. At the heart of this system is the interaction of the two-level atom and the cavity mode. Since the optical resonators used in these systems are of small mode volume and of high finesse $\mathcal{F}$ (or alternatively high quality factor Q), we can ensure that even single quanta

of cavity excitation will have large effects on the atom and that this interaction is long lived. Modelling this interaction, we can approximate it using a simple dipole Hamiltonian where $\hat{d}$ is the atomic dipole operator and $\hat{E}$ is the electric field operator:

$$\hat{H}_{int} \propto \hat{d} \cdot \hat{E} \tag{2.1}$$

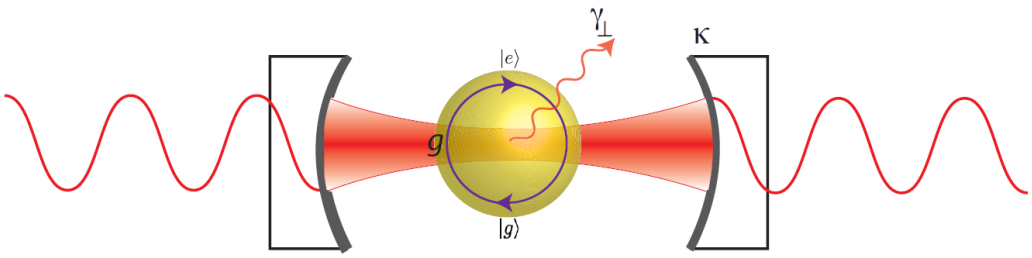

Figure 2.1: Illustration of two-level system coupled to cavity mode within driven optical resonator. Atom and cavity are coupled at a rate g with dissipation out of the system via the spontaneous emission rate $2\gamma_\perp$ and the cavity field decay rate κ.

For a single photon, we use the electric field magnitude

$$E_0 = \sqrt{\frac{\hbar\omega}{2\epsilon_0 V_m}} \tag{2.2}$$

where ω is the optical frequency and V_m being the cavity mode volume. Using this, we can see that the maximum interaction strength between the atom and cavity mode is given by:

$$\hat{H}_{int} = d\sqrt{\frac{\hbar\omega}{2\epsilon_0 V_m}} \tag{2.3}$$

From this we get our first cavity QED parameter g_0 defined as:

$$g_0 \equiv \frac{dE_0}{\hbar} = d\sqrt{\frac{\omega}{2\hbar\epsilon_0 V_m}} \tag{2.4}$$

This is called the atom-field coupling constant, which is the rate at which the cavity mode and the atom are coherently exchanging energy. The remaining two cavity QED parameters come into play in the dissipation mechanisms of the system. The first mechanism is the spontaneous emission of the atom into free space, occurring at a rate $\gamma_{\parallel} = 2\gamma_{\perp}$. The second loss mechanism is the escape of photons out of the cavity mode through the mirrors and other absorptive means, occurring at the total cavity energy decay rate 2κ. Using just these three parameters, $(g_0, \kappa, \gamma_{\perp})$, you are able to fully specify your cavity QED system.

In previous sections, we have talked about how we need a strong nonlinear integration between atom and cavity mode in order to see interesting dynamics in the low energy or quantum regime. Quantitatively we can specify this strong coupling regime in the limit where $g_0 \gg \kappa, \gamma_{\perp}$. In this case, the rate at which the coherent energy exchange between the atom and cavity mode is much larger than any of the loss channels, leading to the strong quantum behavior. You can read the thesis of Michael Armen [14] for a more comprehensive discussion on the topic of qualitatively inferring the influence of the atom onto the cavity mode.

Looking at this system in a more quantitative way, we use the driven Jaynes-Cummings Hamiltonian which models quantum mechanical behavior of this system. We have an optical cavity, with resonant frequency ω_c, a two-level system (an atom in our case) with its ground state $|g\rangle$ and excited state $|e\rangle$ separated by frequency ω_a. The cavity system and two-level system are then coupled to each other, with the atom-field coupling rate g_0. Lastly, the system is driven by a probe field of frequency ω_p with amplitude $\mathcal{E}$. Putting this all together, we get the JC Hamiltonian:

$$\hat{\mathcal{H}} = \omega_c \hat{a}^\dagger \hat{a} + \omega_a \hat{\sigma}^\dagger \hat{\sigma} + i g_0 (\hat{a}^\dagger \hat{\sigma} - \hat{a}\hat{\sigma}^\dagger) + i\mathcal{E}(e^{-i\omega_p t}\hat{a}^\dagger - e^{i\omega_p t}\hat{a}) \tag{2.5}$$

We have used the notation with $\hbar = 1$ and will continue to do so throughout the rest of the thesis. The optical field operator is $\hat{a}$ and atomic lower operator is $\hat{\sigma} = |g\rangle \langle e|$

In order to simplify this equation a bit, we will transform it into a rotating frame to remove the time dependence on the driving term. This can be accomplished using the transformation for the state:

$$\hat{T} = e^{-i\omega_p t \hat{a}^\dagger \hat{a}} e^{-i\omega_p t \hat{\sigma}^\dagger \hat{\sigma}} \tag{2.6}$$

We can now evolve our transformed state under the new Hamiltonian

$$\hat{\mathcal{H}} \rightarrow \hat{T}^\dagger \hat{\mathcal{H}} \hat{T} + i \frac{\partial \hat{T}^\dagger}{\partial t} \hat{T} \equiv \hat{H} \tag{2.7}$$

Apply this to our original Hamiltonian, we get the new transformed Hamiltonian $\hat{H}$ as

$$\hat{H} = \hat{H}_{JC} + \hat{H}_d = \Theta \hat{a}^\dagger \hat{a} + \Delta \hat{\sigma}^\dagger \hat{\sigma} + i g_0 (\hat{a}^\dagger \hat{\sigma} - \hat{a}\hat{\sigma}^\dagger) + i\mathcal{E}(\hat{a}^\dagger - \hat{a}) \tag{2.8}$$

Here, the first two terms are the transformed undriven JC Hamiltonian and the last term is the modified time independent drive term. In addition, we have $\Theta = \omega_c - \omega_p$ as the cavity-probe detuning and $\Delta = \omega_a - \omega_d$ as the atom-probe detuning. For a more rigorous and complete overview of this transformation, please refer to the thesis work of Michael Armen [14].

2.1.1 Adding in dissipation

We have a description for our quantum system but this is not yet complete. As previously discussed, quantum systems that we encounter in the lab do not evolve freely in a closed environment under Schrodinger's equation. We have open quantum systems which are inherently coupled to their environment. In our specific system, we have multiple loss channels which must be taken into account in order to get the full picture. We utilize the master equation (or Lindblad equation) to study the non-unitary evolution of the joint atom-cavity density operator $\hat{\rho}$. In our specific case of two loss channels of decay out of the cavity mirrors (κ) and spontaneous emission out to free space ($\gamma_\perp$), we get the following equation:

$$\dot{\hat{\rho}} = -i[\hat{H}, \hat{\rho}] + \kappa(2\hat{a}\hat{\rho}\hat{a}^\dagger - \hat{a}^\dagger\hat{a}\hat{\rho} - \hat{\rho}\hat{a}^\dagger\hat{a}) + \gamma_\perp(2\hat{\sigma}\hat{\rho}\hat{\sigma}^\dagger - \hat{\sigma}^\dagger\hat{\sigma}\hat{\rho} - \hat{\rho}\hat{\sigma}^\dagger\hat{\sigma}) \tag{2.9}$$

where $\hat{H}$ is our Hamiltonian in the rotating frame.

2.1.2 Semiclassical equation of motion

In practice, it is actually quite difficult to do full master equation quantum simulations of systems of even moderate complexity. The size of the problem grows exponentially and you can really only look at a handful of simple cases. We must turn to an approximate method of analyzing systems in which the full quantum mechanical description is not tractable computationally. We can compute operator expectation values using:

$$\frac{d\langle\hat{O}\rangle}{dt} = \langle\hat{O}\dot{\hat{\rho}}\rangle \tag{2.10}$$

Using equation 2.10 and the master equation from equation 2.9, we get the following equations of motion of the operator expectation values:

$$\begin{aligned}
\frac{d\hat{a}}{dt} &= -(\kappa + i\Theta)\langle\hat{a}\rangle + g_0\langle\hat{\sigma}\rangle + \mathcal{E} \\
\frac{d\hat{\sigma}}{dt} &= -(\gamma_\perp + i\Delta)\langle\hat{\sigma}\rangle + g_0\langle\hat{a}\hat{\sigma}_z\rangle \\
\frac{d\hat{\sigma}_z}{dt} &= -2\gamma_\perp(\langle\hat{\sigma}_z\rangle + 1) - 2g_0(\langle\hat{a}^\dagger\hat{\sigma}\rangle + \langle\hat{\sigma}^\dagger\hat{a}\rangle)
\end{aligned} \tag{2.11}$$

where $\hat{\sigma}_z = [\hat{\sigma}^\dagger, \hat{\sigma}] = |e\rangle\langle e| - |g\rangle\langle g|$ is the the Pauli-z operator, a measure of the difference of the atomic population. Equation 2.11 is traditionally referred to as the Maxwell-Bloch Equations (MBE). These three coupled equations are already looking promising in terms of computation. However if you haven't already noticed, there is one wrinkle. Some of the terms within the equations are dual-operator expectation values, e.g., $\langle\hat{a}\hat{\sigma}_z\rangle$. We are not totally out of luck, we can make some approximations in special circumstances and get away without introducing significant errors. If we factor all three of the dual-operator expectation value terms, e.g., $\langle\hat{a}\hat{\sigma}_z\rangle \rightarrow \langle\hat{a}\rangle\langle\hat{\sigma}_z\rangle$, our set of couple equations now become easily solvable. But before quickly moving onto solving the MBE, let's take a step back and analyze what approximation we really made. By approximating the dual-operator exception value terms by factoring the individual terms, we are essentially inferring that atom-field correlations are not of any significant effect. In cases where there is not much coherent energy exchange ($g_0 \ll \kappa, \gamma_\perp$) relative to the loss mechanisms or in the case of the bad cavity limit ($\kappa \gg g_0 \gg \gamma_\perp$), we can get away with making such an approximation. Thus it is obvious that in the strong coupling regime of cavity QED ($g_0 \gg \kappa, \gamma_\perp$), the solution obtained from the master equation (2.9) and the MBE (2.11) will not match.

To make it easier to work with the MBE, the equations are commonly normalized such that $z \equiv \langle \hat{a} \rangle$, $v \equiv 2\langle \hat{\sigma} \rangle$, $m \equiv \langle \hat{\sigma}_z \rangle$. These substitutions lead to equation 2.11 becoming:

$$\begin{aligned} \dot{z} &= -\kappa(1 + i\theta)z + (g_0/2)v + \mathcal{E} \\ \dot{v} &= -\gamma_\perp(1 + i\Lambda)v + 2g_0 z m \\ \dot{m} &= -2\gamma_\perp(m + 1) - 2g_0(z^* v + v^* z) \end{aligned} \tag{2.12}$$

with $\theta = \Theta/\kappa$ and $\Lambda = \Delta/\gamma_\perp$. Bear with me, we will now go even one step further to get the equations in a more computationally practical form. We will make a change of variables:

$$z \to \sqrt{n_0}x, \quad v \to \sqrt{2}p, \quad m \to -D \tag{2.13}$$

where $n_0 = \gamma_\perp^2/(2g_0^2)$. Additionally we will scale the time such that

$$t \to t^{'}/\gamma_\perp \tag{2.14}$$

This leads us to the dimensionless MBE:

$$\begin{aligned} \dot{x} &= -k[(1 + i\theta)x + 2Cp - y] \\ \dot{p} &= -(1 + i\Lambda)p + xD \\ \dot{D} &= -2[D - 1 + (x^* p + p^* x)/2] \end{aligned} \tag{2.15}$$

were we have $k = \kappa/\gamma_\perp$, $C = g_0^2/(2\kappa\gamma_\perp)$, and $y = \mathcal{E}/(\kappa\sqrt{n_0})$.

Looking at analysing these set of equations, we can easily compute the steady-state solutions. We result in the simple set of solutions in such a case:

$$\begin{aligned} y &= x_{ss}\sqrt{\left[1+\frac{2C}{1+\Lambda^2+|x_{ss}|^2}\right]^2+\left[\theta-\frac{2C\Lambda}{1+\Lambda^2+|x_{ss}|^2}\right]^2} \\ p_{ss} &= \frac{(1-i\Lambda)x_{ss}}{1+\Lambda^2+|x_{ss}|^2} \\ D_{ss} &= \frac{1+\Lambda^2}{1+\Lambda^2+|x_{ss}|^2} \end{aligned} \tag{2.16}$$

2.1.2.1 Many atom MBE

If our system contains more than one two-level atom, we can easily extend our equations to adjust for the situation. When we have N non-interacting atoms all coupled to a cavity-mode, we can write the overall Hamiltonian in the rotating frame as:

$$\hat{H} = \Theta\hat{a}^\dagger\hat{a} + \sum_{j=1}^{N}\Delta\hat{\sigma}_j^\dagger\hat{\sigma}_j + \sum_{j=1}^{N} ig_j(\hat{a}^\dagger\hat{\sigma}_j - \hat{a}\hat{\sigma}_j^\dagger) + i\mathcal{E}(\hat{a}^\dagger - \hat{a}) \tag{2.17}$$

Applying the same methods as done previously to obtain the semiclassical equations of motion. If we assume that each atom has a different coupling strength such that

$$g_j = c_j \cdot g_0 \qquad (j = 1, 2, 3, ..., N) \tag{2.18}$$

The normalized multi-atom MBE become

$$\begin{aligned}\dot{x} &= -k[(1+i\theta)x + 2\sum_{j=1}^{N} c_j C_0 pj - y] \\ \dot{p}_j &= -(1+i\Lambda)p_j + c_j x Dj \\ \dot{D}_j &= -2[D_j - 1 + c_j(x^* p + p^* x)/2]\end{aligned} \tag{2.19}$$

And similarly the steady-state solutions to the equations become

$$\begin{aligned}y = x_{ss}\sqrt{\left[1+\sum_{j=1}^{N}\frac{2c_j^2 C_0}{1+\Lambda^2+c_j^2|x_{ss}|^2}\right]^2 + \left[\theta - \sum_{j=1}^{N}\frac{2c_j^2 C_0\Lambda}{1+\Lambda^2+c_j^2|x_{ss}|^2}\right]^2} \\ p_{j_{ss}} = \frac{(1-i\Lambda)c_j x_{ss}}{1+\Lambda^2+c_j^2|x_{ss}|^2} \\ D_{ss} = \frac{1+\Lambda^2}{1+\Lambda^2+c_j^2|x_{ss}|^2}\end{aligned} \tag{2.20}$$

2.1.3 Examples of nonlinear dynamics in cavity QED systems

Now that we have the quantum and semiclassical equation for both the single atom and multi atom cases, lets explore the types of dynamics we get from the solutions. The most correct thing to do would be a full quantum master equation simulation for every case but as previously stated, such a task is not feasible with the computational power we currently have. For a system which consists of N atoms and a truncated fock basis of size M, our combined state space is of size $M \cdot 2^N$ and density matrix of size $M^2 \cdot 2^{2N}$. It is clear how solving a full quantum model of an arbitrary sized system can get out of hand. We don't have the necessary computer power and also RAM size available to simulate any system that is larger than a couple of atoms.

We will look at two distinct examples: first a strongly coupled single atom and then a large ensemble of weakly coupled atoms. One interesting thing to look at is how the dynamics are different even though the effective linearity in the system is the same. In Equation 2.15 we introduced the constant $C = g_0^2/(2\kappa\gamma_\perp)$, called the cooperativity. This constant includes all the relevant cavity QED parameters into one metric thus giving us a sense of how strong the nonlinear response of the system will be. In the case where you have N atoms all coupled to the cavity mode with equal atom-cavity coupling constant g', we can write the total cooperativity as $C' = Ng'^2/(2\kappa\gamma_\perp)$. When you have $g' = g_0/\sqrt{N}$, the effective nonlinearity of the system, and if we were to just use the semiclassical model for both systems, we would get the exact same solution. However in reality, the quantum solution for the strongly coupled case will not match the semiclassical and thus give different dynamics.

2.1.3.1 Quantum model

So to start off, let's say we have a cavity QED system parametrized by $(g_0, \kappa, \gamma_\perp) = (10, 1, 2.6)\ MHz$. Be careful that all the frequencies used within the quantum optical equations are angular frequencies, so remember to always multiply by 2π. We are definitely in the strong coupling regime in this situation since $g_0 \gg \kappa, \gamma_\perp$ and thus quantum effects are very important. We must use the master equation to solve for the steady state behavior of such a system with constant drive probe amplitude. The quantum optics simulation in this case was done using the Python package QuTiP [21]. After solving for the steady state density matrix, we can visualize the result by plotting the Q function quasi-probability distribution.

The Q functions are a good tool to visualize the quantum state of a quantum optical system.

Looking at the result of the simulation in Figure 2.2, we have quite an interesting looking distribution. For this simulation, we drove the system with probe amplitude $\mathcal{E} = \sqrt{20.2}\kappa$ and all the detunings set to zero ($\Theta = \Delta = 0$). If we had no atom within the cavity, we would just have a 2D gaussian distribution centered around $|\alpha\rangle = \mathcal{E}/(\kappa + i\Theta)$. Our solution is much more interesting than a boring simple gaussian, we have strong bimodal behaviour here. Even with a constant drive two stable states exist, let's call them the *low* state and the *high* state. Without any noise, this system would work perfectly as a binary switch, allowing you to jump between two states with small perturbations of the drive field. But we do not live in a perfect world. The *high* state lives at approximately an intracavity photon number of ≈ 9. With such a low photon cavity mode, quantum fluctuations are on the same order and will cause the system to spontaneously switch.

If we look at a quantum trajectory simulation, we can get a sense of single shot time dependent dynamics of our system. Figure 2.3 clearly shows that with the constant drive to the system we do not get a stable output of $Re[\alpha] = (\hat{a}^\dagger + \hat{a})/2$. The system is jumping back and forth between two distinct stable states due to the spontaneous switching brought upon by quantum fluctuations.

2.1.3.2 Semiclassical model

Now, let's take the exact same model we looked at just now and try to analyze it using the semiclassical MBE. We already argued that since it is in the strong coupling

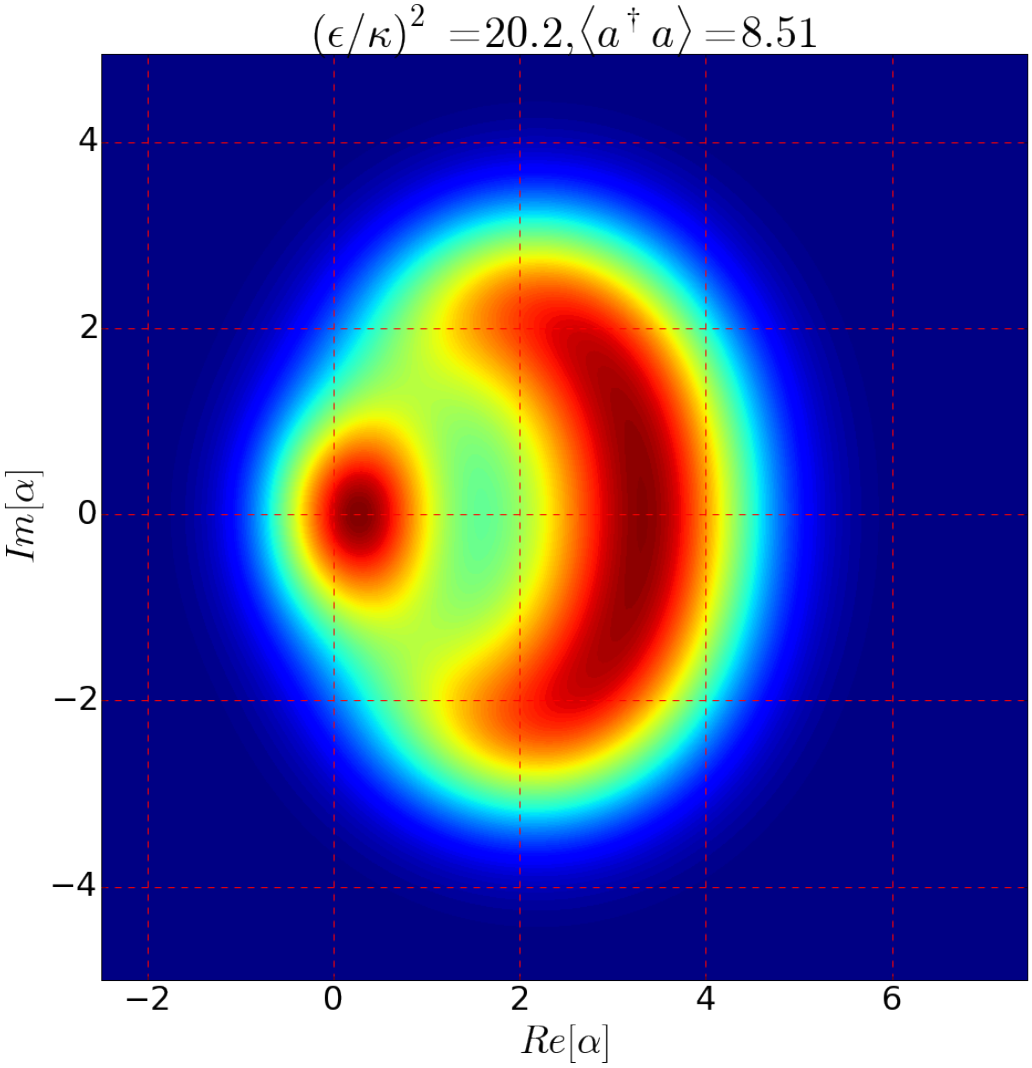

Figure 2.2: Q function of a single atom cavity QED system exhibiting strong bistable response. Our system parameters are $(g_0, \kappa, \gamma_\perp) = (10, 1, 2.6)MHz$ and $(\mathcal{E}/k, \Theta, \Delta) = (\sqrt{20.2}\kappa, 0, 0)$

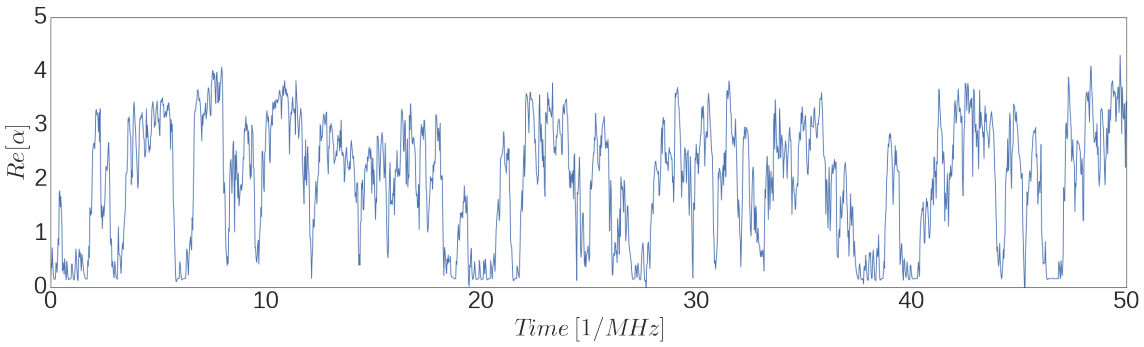

Figure 2.3: Quantum trajectory simulation showing spontaneous switching between two states.

regime, the solution from the MBE will not be correct.

By looking at Figure 2.4, what we notice is that the MBE do predict a bistable response but the drive at which this bistable response occurs is incorrect. The MBE show that the system exhibits bistable response when approximately driven such that $5.5 < (\mathcal{E}/\kappa)^2 < 14$. From the master equation simulation, our system showed bistability when $(\mathcal{E}/\kappa)^2 = 20.25$. This is just one example where the quantum model and semiclassical model do not agree. As you get into the regime of a few atoms, the difference becomes much more apparent until you start converging back together in a many weakly coupled atom system.

Let's say we have atom number $N_{atom} = 2500$. All the atoms are coupled with the exact same coupling constant $g' = 10/\sqrt{2500} = 0.2MHz$. We scaled the coupling constant of each atom according such that the total cooperativity still remains constant at $C = 19.2$. Since the cooperativity is the same between the single atom and the many atom case, the behavior of the nonlinear response will be identical. Figure 2.5 shows the response and it looks identical to the curves in Figure 2.4 except for the fact that the energy levels which the interesting response occurs at is

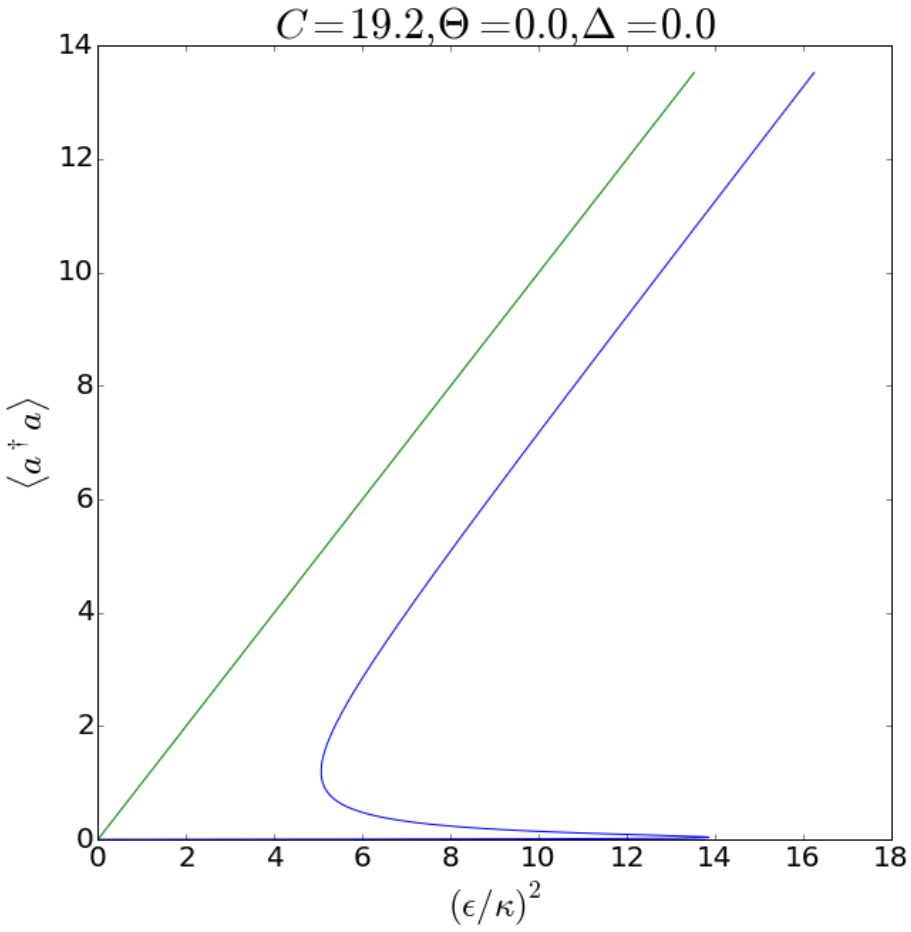

Figure 2.4: MBE simulation of a single strongly coupled atom. Green trace shows the empty cavity response of the system and the blue trace shows the nonlinear response with the atom present.

significantly higher in this many atom case.

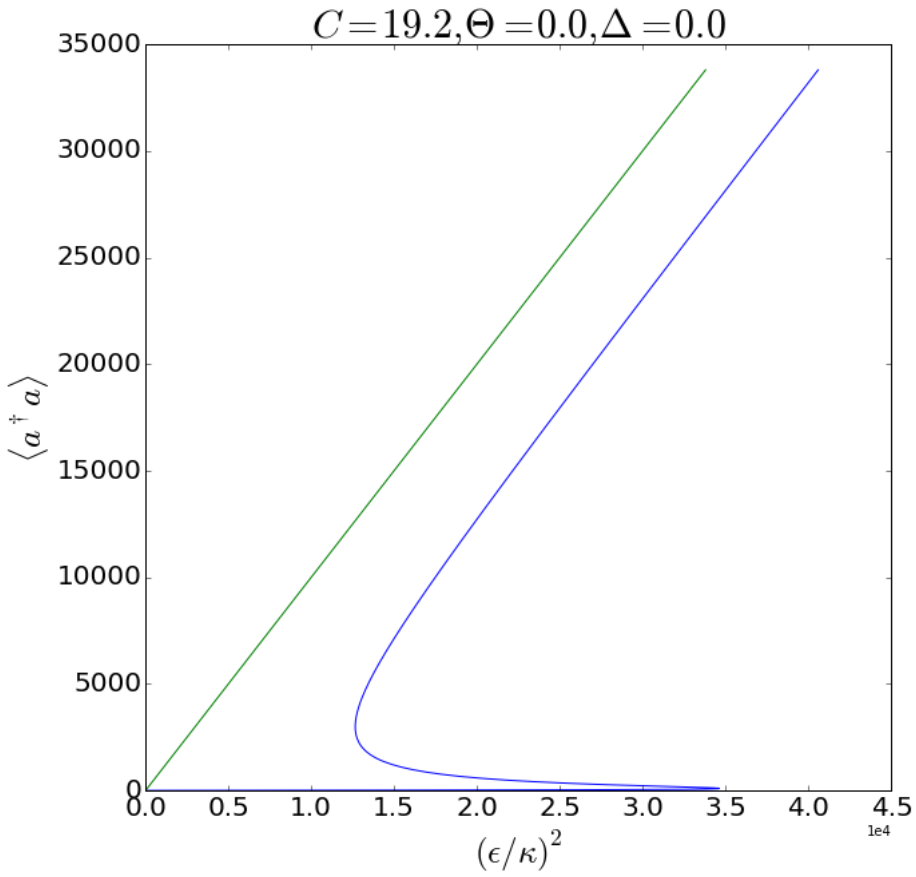

Figure 2.5: MBE simulation of a 2500 weakly coupled atoms. Each atom's coupling strength is 50 times less as compared to the single atom case. We see the same qualitative behaviour but it occurs at a completely different energy regime. Green trace shows the empty cavity response of the system and the blue trace shows the nonlinear response with the atom present.

One question that really troubled me in the beginning of my grad school career was intuitively why does an atom cause a hysteretic response of the input/output like we have seen in our simulations. The atom can be thought of as a dipole and that dipole emits radiation when it transitions from an exited to ground state. Lets

say this dipole lives within an optical cavity. When you start probing the cavity with an input field, the dipole is absorbing the radiation and the field it re-radiates is 180° out of phase from your probe. This cancelling effect never lets the field build up within the cavity and thus suppressing the response. However, since the atom is a saturable absorber, at some point when you keep increasing the drive it just cannot cancel out the field and you have a runaway effect where the intracavity field quickly builds up due to the positive feedback effect of the cavity. Now when you bring the drive back down from a high state to zero, your cavity already has a large field built up inside thus making the atom saturated. Since even small probe levels equal to a large intracavity field, this response stays the same until you get low enough where the atom is no longer saturated and can start its cancelling effect, thus suppressing the field once again. This is the intuition as to why bistability and hysteric behavior can be seen when you have a saturable absorber with an optical cavity [11].

We have now looked at cases of absorptive bistability as it related to systems of a single strongly coupled atom and also systems where you have many weakly coupled atoms. You may wonder why we are so interested in such a response. A system such as this can easily be used as a binary switch, a basic building block of classical information processing devices. If the energy scales at which this switch is occurring is lower or comparable to our modern day electronics, it becomes of great interest for ultra lower power schemes. From a practical standpoint, it will be very difficult to construct system which contain single quantum emitters. What we might want to look at is the regime where say you have a handful of atoms, most of them coupled weakly to the cavity mode and a few coupled strongly. The overall nonlinearity is still large and you see dynamics at a low power regime. You can also translate such a

system to the solid state devices where you will always have some weak background effect superimposed on top of your strong quantum emitter. Modelling such systems still pose a challenge. It would be near impossible to do a master equation simulation for say 20 atoms but the atom number and energy scales are still low enough such that a semi-classical description will not fully capture the dynamics. This regime, call it the mesoscopic regime, is of great research interest to us.

2.2 Quantum Networks

Single devices may exhibit interesting behaviour but the true power lies in the ability to combine a large number of these devices in a network to achieve a much richer and complex response. It might seem like a daunting task to look at complicated networks and think about how to write down a mathematical model to analyze them. Luckily, there have been recent advancements in the field of quantum networks which provide us with powerful tools to approach this exact problem.

2.2.1 SLH formalism

In the Quantum Stochastic Differential Equation (QSDE) framework [9][22], individual open quantum system can be parametrized using a triplet $(\mathbf{S}, \mathbf{L}, \hat{H})$. The scattering matrix $\mathbf{S}$ encompasses the direct scattering of input signals to output signals. The coupling vector $\mathbf{L}$ shows how each external field couples to the integral degrees of freedom of the system. The Hamiltonian H governs the internal dynamics of system. From this parameter set, we can for example directly obtain the Lindblad master equation for our system.

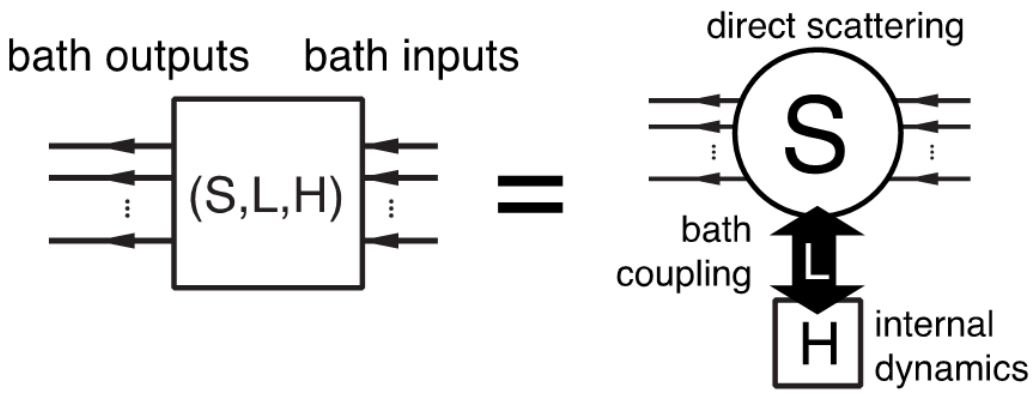

Figure 2.6: An individual quantum network component showing how each term of the parametrization fits into the overall system.

$$\dot{\rho}(t) = \mathcal{L}\rho = -i[H, \rho] + \sum_k \left[L_k \rho L_k^\dagger - \frac{1}{2}\{L_k^\dagger L_k, \rho\} \right] \tag{2.21}$$

Now let's say we have two systems and for each we know their parametrization and mathematical model. If we were to combine the two together in some sort of network configuration, how does the overall system now look? This is exactly what the Gough-James algebra rules [23][24]of the SLH formalism allows us to do. There are three basic circuit operations for networks: concatenation, series connection, and feedback (Figure 2.7)

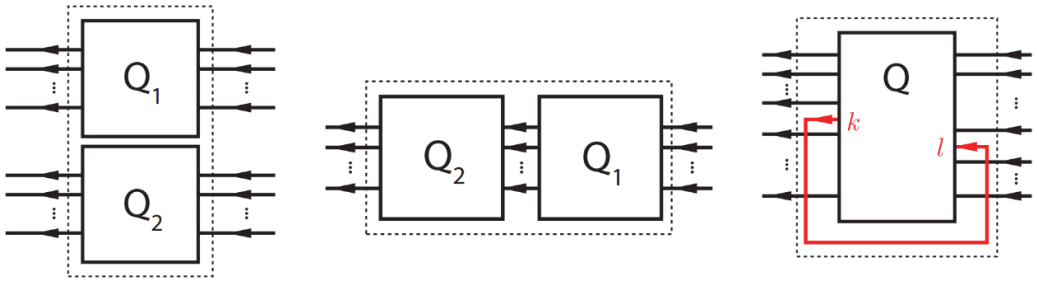

Figure 2.7: Basic network operations in the SLH formalism. First shows concatenation. The second is a series product. The third is a feedback operation.

For each of these operations, there is a systematic approach to how to get a combined

$(\mathbf{S}, \mathbf{L}, \hat{H})$ triplet for the overall system. I will leave the messy details out and refer you to look them up in the thesis work of Nikolas Tezak [25].

2.2.1.1 Quantum hardware description language

To automate this modelling process, Nikolas Tezak in our lab has developed a suite of software tools to easily describe and simulate complex quantum networks. The quantum hardware description language [26] is analogous to the classical VHSIC Hardware Description Language (VHDL) which is extensively used to describe complex digital circuits. We can define individual components and how the inputs and outputs connect together and QHDL will come back with overall models for your system. This is a very powerful tool as it allows engineers and designers to know focus on topologies and architecture using quantum circuits rather than the nitty-gritty quantum physics of each individual element.

2.2.2 Examples of networks in quantum optics

So far we have discussed the properties and dynamics of single quantum optical systems. By applying the methodologies discussed in the previous section about quantum networks, we can now work our way towards looking at interesting complex quantum devices that can be used to perform simple information processing tasks.

The first example [27] we will discuss is an absorptive bistability system in which quantum noise leads to unwanted fluctuations of the bistable state when driven with a constant probe. The system by itself consists of a kerr nonlinear material which provides the necessary optical nonlinearity to see bistable behavior. When driven

with a constant probe such that two stable states exist for the intracavity field, in absence of any quantum fluctuations we should measure a stable output depending on which side we approached the bistable regime. However, as seen in Figure 2.8, the intracavity field shows clear spontaneous switching.

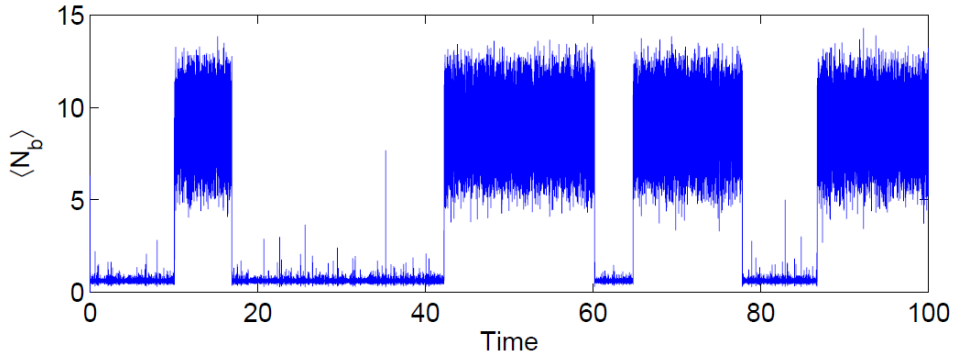

Figure 2.8: Trajectory simulation showing absorptive bistable behavior of the intracavity photon number in kerr nonlinear cavity. [27]

We have this quantum device which exhibits desirable dynamics at very low energy levels but is hampered by these pesky quantum fluctuations making it not robust enough for practical use. This is a situation where application of a quantum network or feedback control will allow us to stabilize the dynamics. Figure 2.9 shows the ring cavity system being wrapped in a feedback network. Two types of feedback are shown to show why complicated nonlinear controllers are required to achieve the sought after control result.

The left setup is taking the output of the system, processing it through a static phase shift, and feeding it back in. The setup on the right does the same but also adds an additional nonlinear phase shift which is dependent on the field amplitude

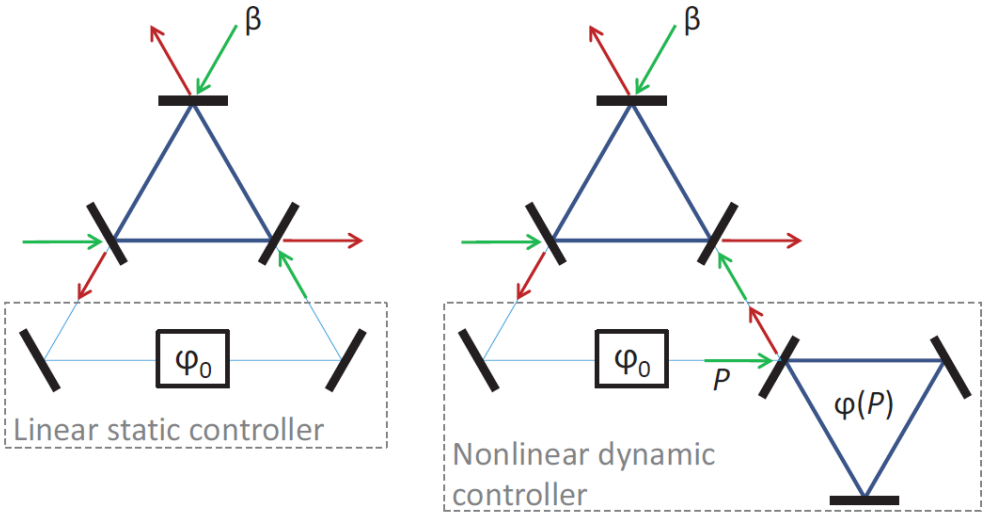

Figure 2.9: Feedback configurations for bistable kerr nonlinear cavity. The static controller does not have the ability to stabilize this system from unwanted quantum fluctuations which cause the state to jump. The nonlinear dynamic controller has the phase of the reflected signal that depends on incident power and thus can be used to stabilize such a system. [27]

reflecting off the second controller cavity. You can easily see how the system on the left will work in what we are trying to achieve. In order to stabilize the spontaneous switching, we will need to stabilize both the high photon number and low photon number state at the exact same time. However, each of two states require the feedback beam to interfere differently at the feedback mirror, constructively for the high state and destructively for the low state. That is why a static controller will never achieve the control goal. With the nonlinear controller, Figure 2.10 shows how the rate of the spontaneous switching at constant probe is greatly reduced in comparison to the open loop case.

Another example of a quantum network, one that more closely resembles an existing classical component, is the all optical nand latch [28]. In this setup (Figure

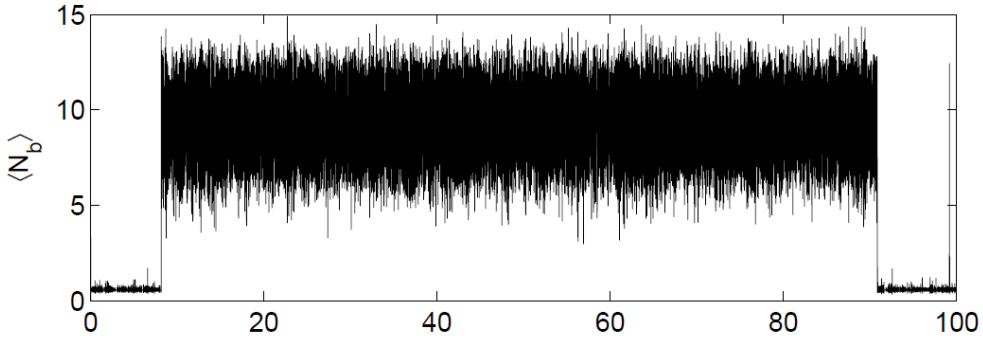

Figure 2.10: Trajectory simulation showing absorptive bistable behavior of the intracavity photon number in stabilized kerr nonlinear cavity. The rate of spontaneous jumping is greatly reduced compared to open loop system. [27]

2.11), we network two components together to construct a one bit memory system. Each of those components is a boolean nand gate. By taking the output of each of the nand gates and feeding them back into the input of the other, we can create a feedback loop which allows us to save a specific output state without having to hold that value at the input. To me, this example is very exciting. If we can construct single boolean gate type devices using an all optical system, that opens up limitless possibilities since all types of boolean algebra operation can be performed by networking nand gates. Obviously to make anything super interesting, we are talking about networking thousands of these devices. Nevertheless it is a start in the right direction.

2.2.3 Self feedback of single cavity system

The quantum optical system of interest for us is a simple Fabry–Pérot cavity setup with atoms coupled to the cavity mode. We have discussed in great detail the methods of modelling such a system and some of the expected dynamics we can

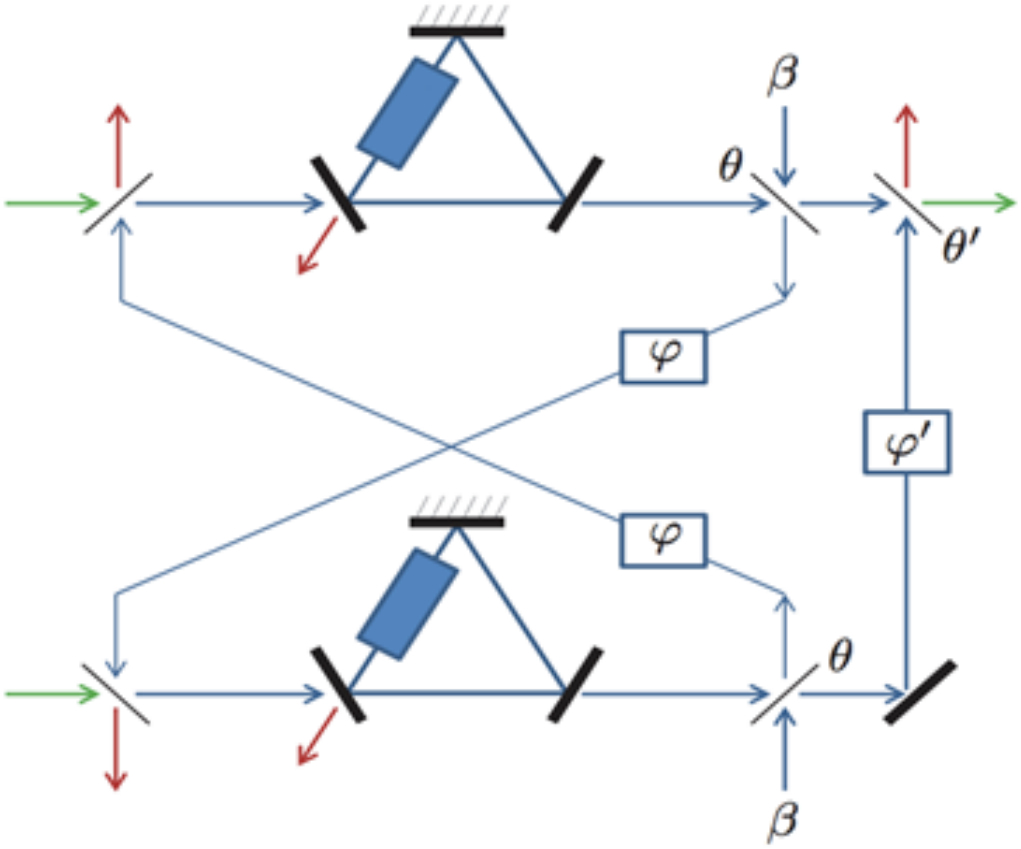

Figure 2.11: All optical nand latch composed of two photonic nand gates in a network configuration. [28]

observe in various parameter regimes. To extend this system with a simple network, we will look at a self-feedback setup as depicted in Figure 2.12.

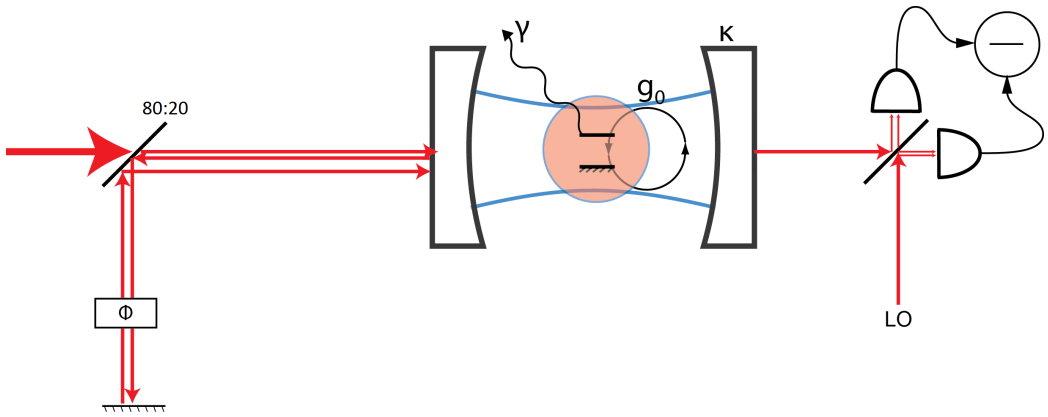

Figure 2.12: Schematic of self-feedback implementation with a Fabry–Pérot cavity. Feedback is applied to the input mirror of the cavity. The feedback phase is statically set via electronic control.

If we want to manually go about writing a model that describes this system, the math will get quite messy. Luckily we have methods and tools available for exactly this. We use the SLH formalism to extract out equations of motion without much effort. Let's set up our system by first considering only the input port of the cavity. The circuit schematic for such a configuration looks as follows:

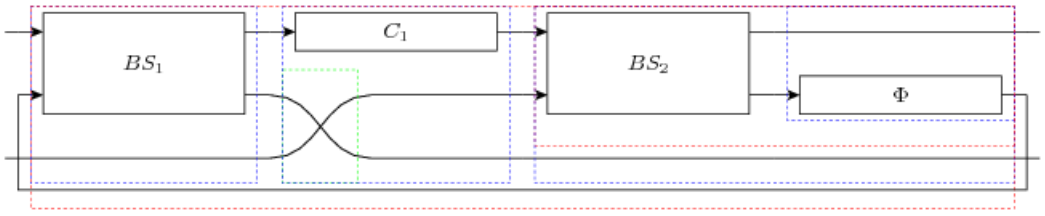

Figure 2.13: Circuit schematic of self-feedback implementation with a single port Fabry–Pérot cavity.

Our system is one that has multiple input and two outputs (you never use some of

the inputs or outputs but there is always an equal number). You can inject probe beams at each port of the beamsplitter before the cavity. Also, a beam can leave our system by escaping back out of the first cavity mirror and also transmitting in reverse through the beamsplitter. For simplification, we model the reverse pass through the beamsplitter with a second beamsplitter element but both have the exact same properties. With the application of feedback, we connect the beam path back into the input mode of the cavity.

Now that we have our feedback mechanism described, we can go ahead and add in the second mirror of the cavity system, the Hamiltonian $\hat{H}$ describing the internal dynamics and the input probe beam. Using the SLH formalism and the Gough-James algebra, we can obtain the overall SLH description. For comparison, we will first write down the SLH model of a simple cavity system with no feedback

$$\left(\begin{pmatrix} 1 & 0 & 0 \\ 0 & 1 & 0 \\ 0 & 0 & 1 \end{pmatrix}, \begin{pmatrix} \alpha + \sqrt{\kappa} a_{\mathrm{fock_{jc1}}} \\ \sqrt{\kappa} a_{\mathrm{fock_{jc1}}} \\ \sqrt{\gamma} \sigma_{\mathrm{g,e}}^{\mathrm{tls_{jc1}}} \end{pmatrix}, -\frac{i\alpha}{2}\sqrt{\kappa} a_{\mathrm{fock_{jc1}}}^{\dagger} + \frac{i\sqrt{\kappa}}{2}\overline{\alpha} a_{\mathrm{fock_{jc1}}} + \Delta \Pi_{\mathrm{e}}^{\mathrm{tls_{jc1}}} \right.$$
$$\left. + \Theta a_{\mathrm{fock_{jc1}}}^{\dagger} a_{\mathrm{fock_{jc1}}} + iga_{\mathrm{fock_{jc1}}}^{\dagger} \sigma_{\mathrm{g,e}}^{\mathrm{tls_{jc1}}} - iga_{\mathrm{fock_{jc1}}} \sigma_{\mathrm{e,g}}^{\mathrm{tls_{jc1}}} \right) \tag{2.22}$$

With a feedback network in place, even one as simple as self-feedback, the equation becomes significantly more complicated. Our SLH model for the feedback setup is

$$\left(\begin{pmatrix} -\frac{\cos^2(\theta)}{e^{i\phi}\sin^2(\theta)-1} & \frac{(-e^{i\phi}+1)\sin(\theta)}{e^{i\phi}\sin^2(\theta)-1} & 0 & 0 \\ \frac{(-e^{i\phi}+1)\sin(\theta)}{e^{i\phi}\sin^2(\theta)-1} & -\frac{e^{i\phi}\cos^2(\theta)}{e^{i\phi}\sin^2(\theta)-1} & 0 & 0 \\ 0 & 0 & 1 & 0 \\ 0 & 0 & 0 & 1 \end{pmatrix}, \begin{pmatrix} -\frac{\epsilon\cos^2(\theta)}{e^{i\phi}\sin^2(\theta)-1} - \frac{\sqrt{\kappa_1}\cos(\theta)}{e^{i\phi}\sin^2(\theta)-1} a_{\text{fock}} \\ -\frac{\epsilon\left(e^{i\phi}-1\right)\sin(\theta)}{e^{i\phi}\sin^2(\theta)-1} - \frac{\sqrt{\kappa_1}e^{i\phi}\sin(2\theta)}{2e^{i\phi}\sin^2(\theta)-2} a_{\text{fock}} \\ \sqrt{\kappa_2}a_{\text{fock}} \\ \sqrt{\gamma}\sigma_{1,0}^{\text{tls}} \end{pmatrix}, \frac{i\epsilon\sqrt{\kappa_1}\left(2e^{i\phi}\cos(\theta)-\frac{1}{2}\cos(\theta)+\frac{1}{2}\cos(3\theta)\right)}{4\left(e^{i\phi}\sin^2(\theta)-1\right)\left(e^{i\phi}-\sin^2(\theta)\right)} a_{\text{fock}}^{\dagger}$$

$$+ \frac{i\epsilon\sqrt{\kappa_1}\left(\left(e^{i\phi}-1\right)\sin(\theta)\sin(2\theta)-2\cos^3(\theta)\right)e^{i\phi}}{4\left(e^{i\phi}\sin^2(\theta)-1\right)\left(e^{i\phi}-\sin^2(\theta)\right)} a_{\text{fock}} + \Delta\Pi_0^{\text{tls}} + \frac{\Theta\left(e^{2i\phi}\sin^2(\theta)-e^{i\phi}\sin^4(\theta)-e^{i\phi}+\sin^2(\theta)\right)-\frac{i\kappa_1}{16}\left(e^{2i\phi}-1\right)(\cos(4\theta)-1)}{e^{2i\phi}\sin^2(\theta)-e^{i\phi}\sin^4(\theta)-e^{i\phi}+\sin^2(\theta)} a_{\text{fock}}^{\dagger}a_{\text{fock}} + iga_{\text{fock}}^{\dagger}\sigma_{1,0}^{\text{tls}} - iga_{\text{fock}}\sigma_{0,1}^{\text{tls}} \Bigg)$$

Using this complex SLH description of our system, we will go about obtaining the Heisenberg equation of motion for the cavity field

$$\frac{\epsilon\sqrt{\kappa_1}\left(4e^{i\phi}\cos(\theta)-\cos(\theta)+\cos(3\theta)\right)}{4\left(e^{i\phi}\sin^2(\theta)-1\right)\left(e^{i\phi}-\sin^2(\theta)\right)}$$
$$+ \frac{1}{e^{2i\phi}\sin^2(\theta)-e^{i\phi}\sin^4(\theta)-e^{i\phi}+\sin^2(\theta)}\left(-i\Theta e^{2i\phi}\sin^2(\theta) + i\Theta e^{i\phi}\sin^4(\theta) + i\Theta e^{i\phi} - i\Theta\sin^2(\theta) - \frac{\kappa_1}{16}e^{2i\phi}\cos(4\theta) + \frac{\kappa_1}{16}e^{2i\phi} + \frac{\kappa_1}{8}e^{i\phi}\sin^2(2\theta) + \frac{\kappa_1}{2}e^{i\phi}\cos^2\right.$$
$$\left.(\theta) + \frac{\kappa_1}{16}\cos(4\theta) - \frac{\kappa_1}{16} - \frac{\kappa_2}{2}e^{2i\phi}\sin^2(\theta) + \frac{\kappa_2}{2}e^{i\phi}\sin^4(\theta) + \frac{\kappa_2}{2}e^{i\phi} - \frac{\kappa_2}{2}\sin^2(\theta)\right) a_{\text{fock}} + g\sigma_{1,0}^{\text{tls}}$$

If we compare this large equation to the equation of motion for a simple cavity with no feedback, we can extract out effective loss, detuning, and drive terms.

$$\dot{a}_{\text{fock}} = -\left(i\Theta + \frac{\kappa_1}{2} + \frac{\kappa_2}{2}\right) a_{\text{fock}} \tag{2.23}$$

Comparing the equations with 2.23, we pull out:

The effective cavity decay rate

$$\kappa_{eff} = -\frac{-\kappa_1 e^{i\phi}\sin^4(\theta) + \kappa_1 e^{i\phi} - \kappa_2 e^{2i\phi}\sin^2(\theta) + \kappa_2 e^{i\phi}\sin^4(\theta) + \kappa_2 e^{i\phi} - \kappa_2\sin^2(\theta)}{e^{2i\phi}\sin^2(\theta) - e^{i\phi}\sin^4(\theta) - e^{i\phi} + \sin^2(\theta)} \tag{2.24}$$

The effective cavity-probe detuning

$$\Theta_{eff} = \frac{0.5i}{e^{2i\phi}\sin^2(\theta) - e^{i\phi}\sin^4(\theta) - e^{i\phi} + \sin^2(\theta)}\Big(-2i\Theta e^{2i\phi}\sin^2(\theta) + 2i\Theta e^{i\phi}\sin^4(\theta) + 2i\Theta e^{i\phi} - 2i\Theta\sin^2(\theta) - \frac{\kappa_1}{8}e^{2i\phi}\cos(4\theta) + \frac{\kappa_1}{8}e^{2i\phi} + \frac{\kappa_1}{8}\cos(4\theta) - \frac{\kappa_1}{8}\Big) \tag{2.25}$$

The effective driving

$$\epsilon_{eff}/\epsilon = -\frac{\sqrt{\kappa_1}\left(4e^{i\phi}\cos(\theta) - \cos(\theta) + \cos(3\theta)\right)}{4\left(e^{i\phi}\sin^2(\theta) - 1\right)\left(e^{i\phi} - \sin^2(\theta)\right)} \tag{2.26}$$

Let's not dwell too much on the complexity of these equations. What we want to get out of all of this is the quantitative dependence of the effects of the feedback phase. Plotting the effective decay rate of the cavity and output rate from the second cavity mirror, we can see that the feedback has profound affects on the behavior of the system and differs tremendously from the no feedback case. A quick correlation we see is that we can map the feedback phase points of $\phi_{fb} = 0$ and $\phi_{fb} = \pi$ to when the measured output of the cavity system is at maximum or minimum. Within our experiment setup, we will explore these characteristics of such a system to verify the control of cavity QED parameters with the application of self-feedback.

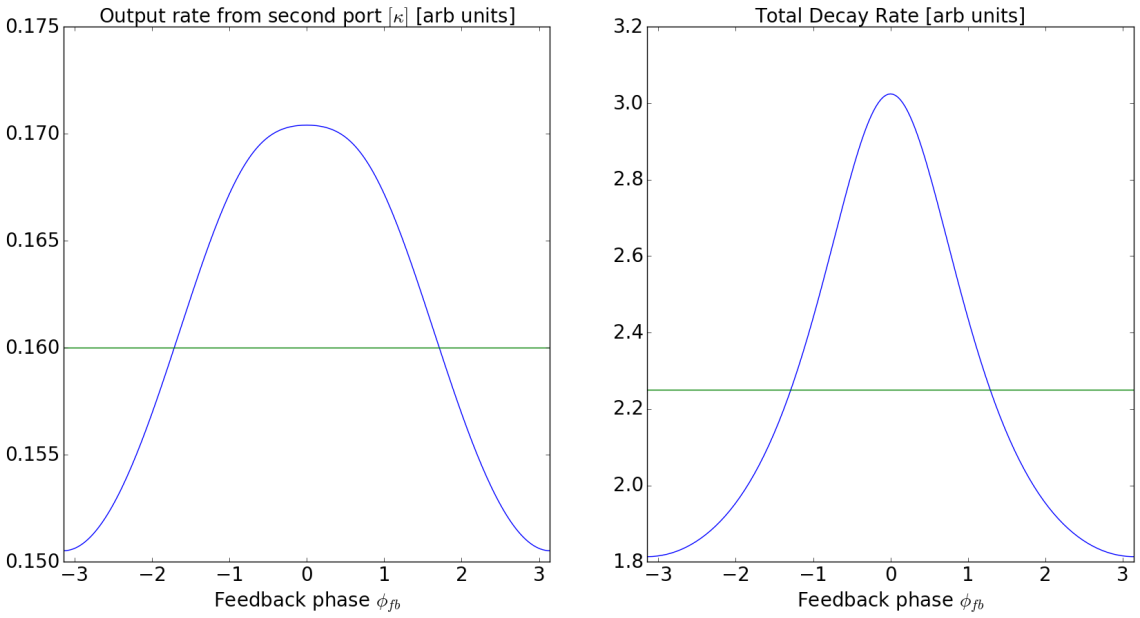

Figure 2.14: Cavity output and effective decay rate as a function of feedback phase in self-feedback configuration. The green trace in each of the plots is the nominal no feedback value for each quantity. Both the output and effective decay rate oscillate with respect to the feedback phase.

Chapter 3

Experimental Setup

In this chapter, we go over the complex tabletop optical setup that was used to perform the experiments. The apparatus can be broken up into three parts: laser system setup, the cavity, and atom preparation and delivery. A cloud of atoms, cesium in our case, is trapped above a Fabry–Pérot cavity with a vacuum chamber by the use of laser cooling and trapping. These atoms are released and fall through the opening of the optical resonator, interacting with a probe as they travel through the cavity mode. A complex laser system in conjunction with a slew of analog electronic are used for the generation of the various laser beams required to lock and probe the system. Measurement on the system is performed using an optical heterodyne setup, allowing us to get near shot noise limited detection.

A vast majority of the optical, mechanical, and electronics setup was from the thesis works of Michael Armen (Mike) [14] and Joseph Kerckhoff (Joe) [29]. The setup has been moved between various cities and buildings and was in the process of being revived in a new building as I was joining the group. I was tasked with bringing

the entire system back to life and making the necessary modifications needed for my specific experiments.

3.1 Laser system setup

At the core of this experimental setup is a complex and dense optics table. My first reaction when I saw such a system was, "how in the world will I ever be able to figure out what every single component does?" The task seems daunting but constantly working with such systems, you quickly learn that they are constructed in a way to be very modular, and debugging them is not as hard as it first seems. Here is my optics setup, as seen in Figures 3.1 and 3.2.

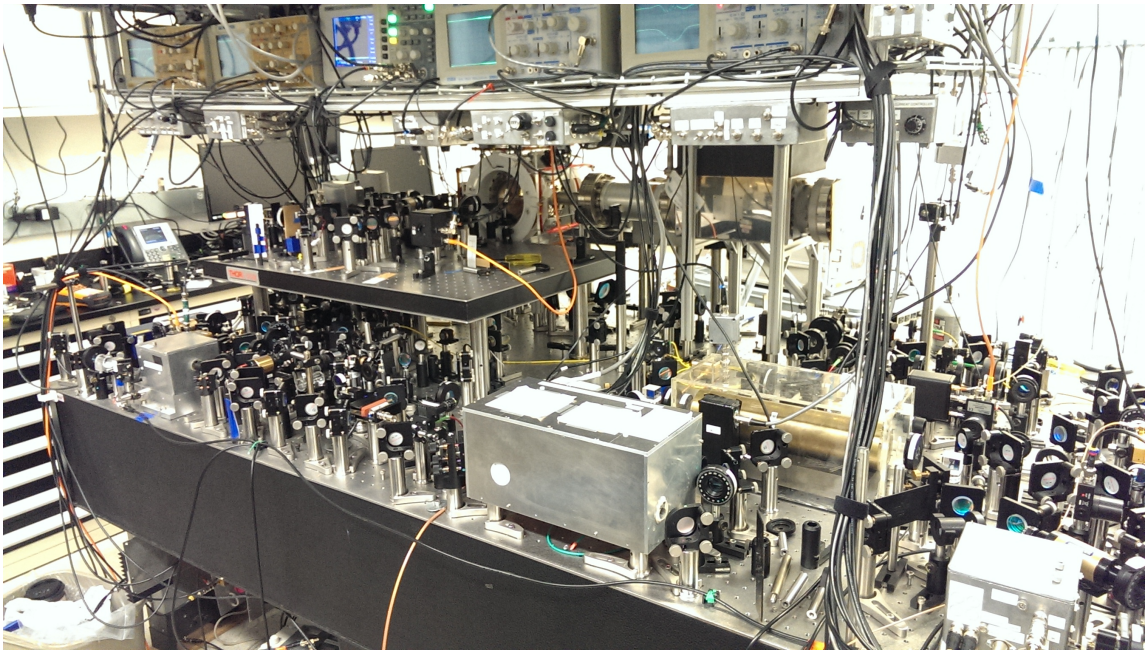

Figure 3.1: This picture illustrates the complexity and density of optics setups for cavity QED systems.

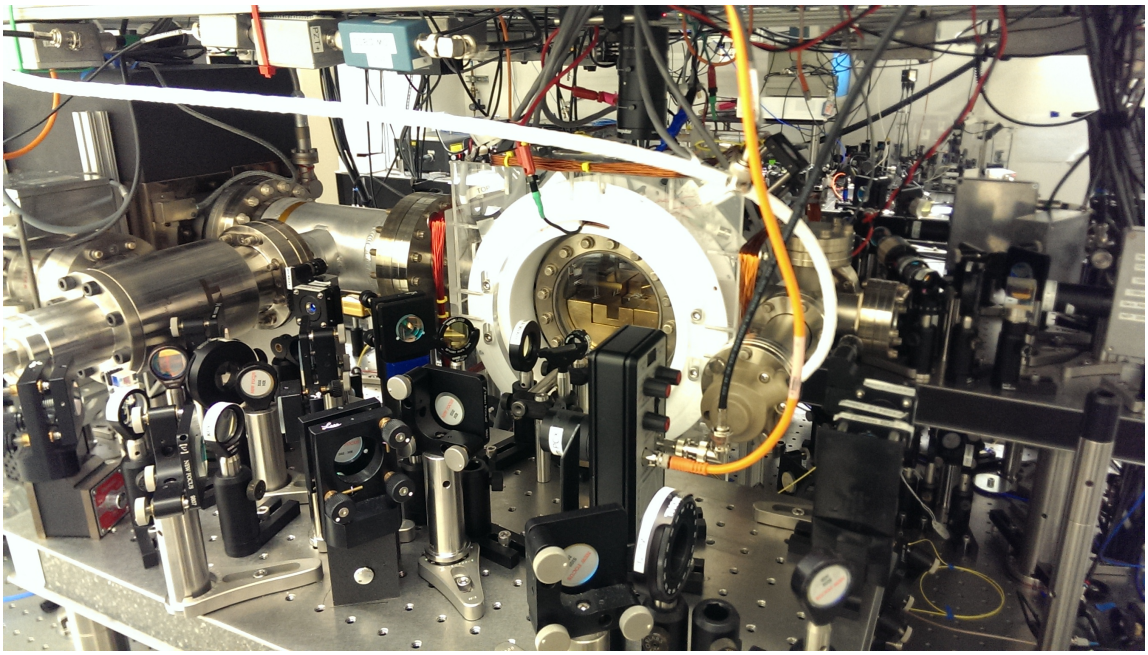

Figure 3.2: This picture illustrates the vacuum chamber and input optics setup.

For completeness, we will now cover the individual optical and electronic components of the setup. The schematic diagram in Figure 3.3 is the same one found in Joe's thesis [29]. Majority of the components remained the same and I was tasked to re-set this up according to this configuration.

The main laser that drives our laser system setup is the fancy Toptica DL Pro which operates at a wavelength of 852nm. It does have a small amount of tunability around that wavelength but we will be using it to probe a very narrow atomic transition in the wavelength range. The beam from the diode laser is first double passed through an acousto-optical modulator (AOM) which shifts the frequency by $-253MHz$ (AOM1 in Figure 3.3). The shifted beam is not put through a transfer cavity. This transfer cavity (TC) is a large mechanically stable 25cm long tabletop cavity. The DL Pro's is locked to the transfer cavity by the use of a

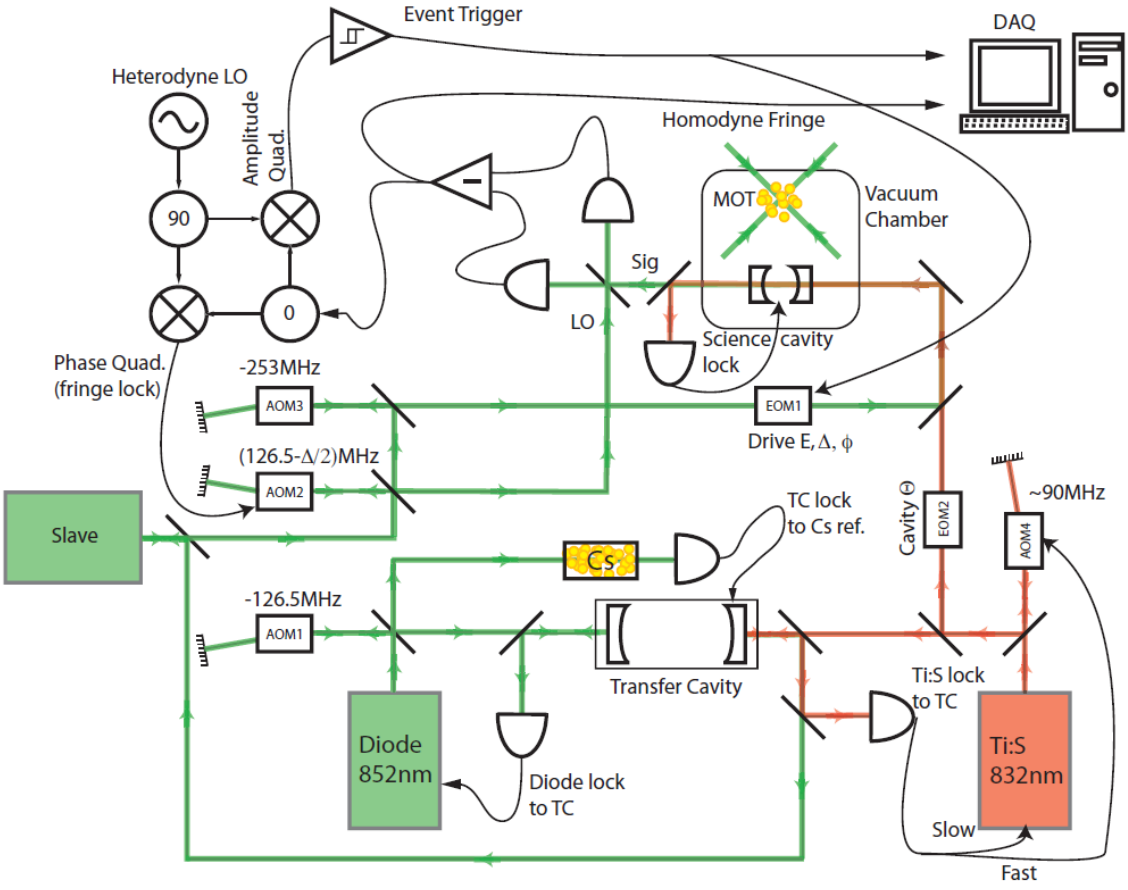

Figure 3.3: Schematic diagram of the major optical and electrical computer in the cavity QED setup.

Pound–Drever–Hall (PHD) technique [30] on the reflected signal, such that the frequency shifted beam is resonant with the TC. The DL Pro has both a fast current feedback port and a slower piezo feedback port. We utilize both in a two-branch servo to lock the laser to the TC. In addition, we send the raw beam from the DL Pro to a cesium cell in a saturated absorption setup. This scheme allows us to lock our TC such that the nominal output frequency of the DL Pro is the frequency of the cesium $F = 4 \rightarrow F' = 5$ D_2 atomic transition.

With our master laser locked, we will use the extremely narrow frequency output beam from the TC to seed an homemade injection locked diode laser. Doing so will provide us with an extremely stable high power source to use in various places within the experimental setup. The output of this slave laser is used for three applications within the experiment: the probe to the science cavity, the local oscillator (LO) beam for our heterodyne measurement setup, and also a seed to produce the beams for the magneto-optical trap.

The component for the probe beam is further frequency shifted by double passing it through another modulator (AOM3) to impart on it an additional frequency shift of $-506MHz$, for the total red shift of $759MHz$. The shifted probe is then sent through a fiber electro-optical modulator (EOM1) to add sidebands to the light. With a tunability range of up to around $1GHz$, we have the significant flexibility in selecting the final probe frequency by setting the EOM frequency.

The component for the LO beam is also again frequency shifted by double passing it through AOM2. However it is blue shifted to bring the frequency back close to the

atomic transition frequency since all of our experiments will be performed in that range. This AOM provides us the flexibility to adjust the LO frequency to match the probe even in situations where the probe beam is detuned from the atomic transition. The LO was setup such that the power available for detection was 2mW.

For the laser cooling and trapping part of the setup, we take a small component of output of the slave laser and send it into a homemade tapered amplifier (TA) to generate the beams. Before seeding the TA, the light is double passed through an AOM to bring the frequency back close to the atomic transition frequency since the output of the slave laser was red detuned by $253MHz$. The amount of light available for the seed is 30mW. The TA used in the setup is quite old and probably running on its last legs. With a lot of effort, we are able to get out just over a 100 mW. That beam is further passed through components, one being another AOM. This static AOM serves a dual purpose by covering the remaining frequency shift in order to get the beam at the appropriate frequency for tapping but also as a fast electronic shutter. The resulting beam is then fiber coupled to the other side of the table to be used in the experiment. Originally, a 2 to 6 fiber splitter was used to combine the trapping beams with the repumper beam (more on this later) and distribute them to the 6 necessary beams needed to form the MOT. However, due to the splitter malfunction, we changed it such that we used 3 beams, one for each axis, and retro reflected them on themselves to achieve the same result.

Now that we have finished covering the 852nm light, we will shift focus to the 825nm laser beam which is used to lock the science cavity in our experiment. This beam is generated using a titanium-sapphire (Ti:S) commercial laser system. The

TiS laser is frequency locked to the TC as well but in the opposite direction. This allows for TiS laser to exactly follow the Toptica DL Pro. Getting the frequency for the TiS just right so that a resonant mode exists in both the science cavity and TC is a bit tricky but there is a lot of flexibility with the wavelength tuning mechanism available to you. In terms of locking the science cavity with this beam, it needs to be resonant with the cavity at the same as the 852nm beam (or close). In order to achieve this flexibility, the locking beam is sent through a fiber EOM to put sidebands on it. These sidebands are adjusted to set the resonant frequency of the cavity. The cavity coatings are also very high reflectors at 825nm, allowing for a sharp resonance. Actual locking of the science cavity is done via a transmission PDH.

3.2 Atom preparation and delivery

At room temperature, a gas of cesium atoms would be whizzing by at speeds over $200m/s$. It would be impossible to controllably get such atoms into a tiny optical resonator to perform experiments. Delivery of the atoms is actually quite controlled. First we start up by forming a magneto optical trap of the cesium atoms about 1 cm above the cavity. In order to even think about laser cooling atoms, we need them to be in an ultra high vacuum environment of about 10^{-7} torr. Traditionally six beams are required to form a MOT but we used only three and retro reflected them onto themselves to get two counter propagating beams for each of the axises. The beams were blown up to have a diameter of around $1cm$ and also $15mW$ of power. We form a quadrapole trap centered at the location of trapping interest with the use of an anti-Helmholtz coil and various smaller Helmholtz coils. The technique for trapping the atoms was quite straight forward; we did not try to do anything more fancy than

a MOT [31][32].

The atoms were sourced via a getter that was located a ways away from the cavity. The output from the getter is directional and you can build up pretty large background pressures with this thing. In the beginning when I could not create a MOT for the life of me, I ran the getter on the highest current setting. This eventually did allow me to find a weak MOT signal and tune from there but it also led to the quick degradation of the cavity. Since the opening of our cavity is large relative to previous cavity QED experiments, we are more susceptible to the background cesium pressure. Over time, cesium atoms stick onto the mirror coatings introducing an additional loss and thus lowering the finesse. When this occurred in my case, I was able to save the cavity by sonicating the mirrors with the high reflector surface facing toward a solution a mild citric acid.

In our vacuum chamber, the geometry of the physical chamber restricts how low you can get the beams to cross over the cavity. The best you can do is around 10-12 mm above the cavity. It would have been nice to get the atoms closer so that they have slower speeds as they propagate through the cavity mode.

3.3 The cavity

The last key component to our cavity QED setup is the high finesse Fabry–Pérot cavity. It is constructed using two spherical high reflectivity mirrors (both with radius of curvature R) which are separated by length l. This leads to a fundamental TEM_{00} Gaussian mode with waist

$$w_0^2 = \frac{z_0 \lambda}{\pi} \tag{3.1}$$

where z_0 is the Rayleigh range of the Gaussian beam. For a symmetric optical cavity, we have

$$z_0 = \frac{l}{2}\sqrt{2\frac{|R|}{l} - 1} \tag{3.2}$$

$$w_0^2 = \frac{\lambda l}{2\pi}\sqrt{2\frac{|R|}{l} - 1} \tag{3.3}$$

Now for our specific setup, the cavity mirrors are separated by $300\mu m$ and have a $10cm$ radius of curvature. At a wavelength of 852nm, we get a mode with Gaussian waist of $32.4\mu m$ and free spectral range $FSR = 500GHz$. We are also interested in calculating the mode volume for our cavity mode since we will need it in determining the coupling coefficient. For the TEM_{00} mode in a cavity of length l, the mode volume is

$$V_m = \frac{\pi}{4} w_0^2 l \tag{3.4}$$

We can now compute the atom-field coupling strength from

$$g_0 = d\sqrt{\frac{\omega}{2\hbar\epsilon_0 V_m}} \tag{3.5}$$

where d is the dipole moment of the atomic transition. We can go ahead and calculate this out for our cavity, giving us a value of $g_0 = 13.2MHz$. We are well on our way to parameterizing our science cavity.

The last thing we need to determine is the cavity decay rate which can be calculated by measuring the cavity linewidth. Measurement of the linewidth is straight forward as it can be done by fitting a Lorentzian function to a frequency swept signal of the cavity transmission or by measuring the cavity decay rate using a ringdown measurement. We can also go about estimating this by first calculating the expected finesse of the cavity. The mirrors used in the formation of the cavity are a $\lambda/4$ dielectric stack on a $10cm$ radius of curvature polish glass surface. These mirrors were custom ordered from Advanced Thin Film (ATF). It is only coating developments of the past two decades that have allowed us to achieve mirror surfaces with such high reflectivities. The mirror coatings are specified to have 8ppm transmission at 852nm and a absorption/scattering loss of 2ppm. We can calculate the finesse of such a cavity using

$$\mathcal{F} = \frac{2\pi}{L_{tot}} = \frac{2\pi}{(T_1 + A_1) + (T_2 + A_2)} \tag{3.6}$$

where L_{tot} is the total round trip loss within the cavity. This gives us a calculated finesse of $\mathcal{F} = 314,000$. Using the finesse and the FSR, we can calculate the linewidth using

$$\mathcal{F} = \frac{FSR}{\delta f} \tag{3.7}$$

With this expression we get a cavity linewidth of $\delta f = 1.6MHz$ and a cavity decay rate $\kappa = \delta f/2 = 0.8MHz$. Lastly, with the fixed spontaneous emission rate of the cesium atom, we now have all our cavity QED parameters $(g_0, \kappa, \gamma_\perp) = (13.2, 0.8, 2.6) \quad MHz$.

3.3.1 Construction of cavity

The cavity which I used for these experiments is a modified version of Joe's cavity from this thesis work [29]. Each mirror is formed from a 5cm diameter cylinder to a bullet shape with the high reflector side of the mirror having a diameter of 2cm. This is done because if you wanted to form a cavity on the order of $10\mu m$, you would not be able to get the mirrors physically that close if they had a diameter of 5cm. Due to the curvature of the mirror surface, the outer edges limit the minimum mirror separation. Since the cavity modes will have beam waits on the order of 10's of microns, it is unnecessary to have mirrors this large. The mirrors are each mounted within aluminum rings. The ring diameter is slightly larger than the mirror's at the point of contact. This was originally done because the mirrors were not glued into the rings but rather held by three 15mil thick strips of RTV655 places symmetrically around the the ring. In Mike's original experiment, the mirrors were glued into their mounts. This glue caused strain within the mirror substrates which propagated to the inside cavity surface. Since you can never perfectly glue the mirror symmetrically around the ring holder, this strain will be uneven. This uneven strain in a high finesse cavity causes significant birefringence. Joe tried to solve this problem by not gluing the mirrors but holding them with friction using rubber strips. The birefringence problem was solved but mechanically stabilizing the length of the science cavity became a nightmare.

When modifying Joe's cavity, I did attempt to use the RTV strip method at first. I experienced far too much mechanical noise and ended up just gluing the mirrors to the ring. Since I wasn't perfect in my gluing technique, significant birefringence returned to the cavity. Continuing with the construction of the cavity, the aluminum

rings are glued down to in a half-pipe shaped slot. Each of these mirror mounts were subsequently glued to a double stack shear mode piezoelectric plate. The piezo stacks where then glued down with conductive epoxy to a H shaped aluminum block sized approximately 5cm by 2cm. Figure 3.4 shows a mechanical drawing and picture of this cavity mount setup.

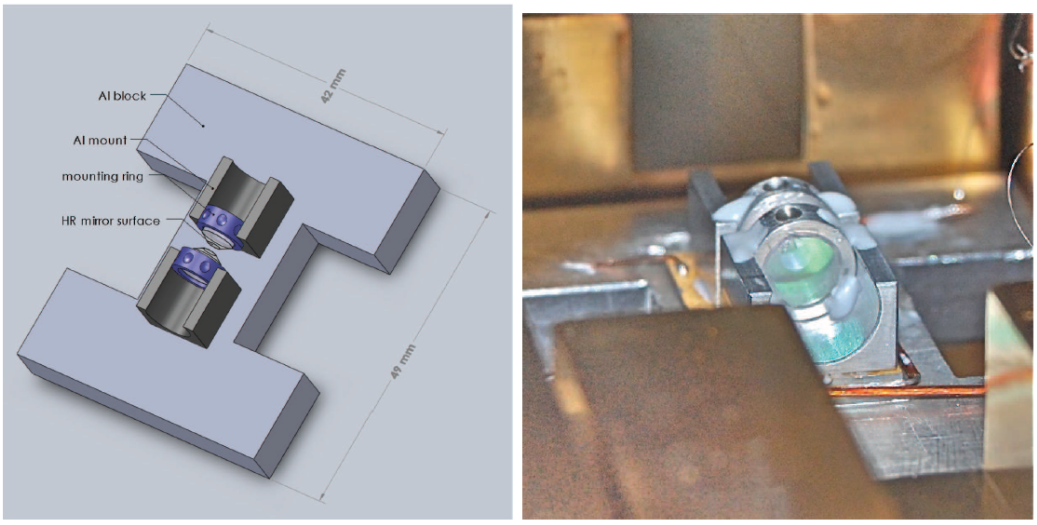

Figure 3.4: Schematic and picture of mount used in the construction of the Fabry-Perot cavity for the experiment.

This cavity mount was ultimately placed upon a multi-stage vibration isolation stack within the vacuum chamber. Doing so decouples the cavity from any mechanical vibrations that creep into the system through the optical table and the vacuum chamber. You can refer to Mike's thesis work [14] for a more detailed description of the isolation stack that he built and I just used.

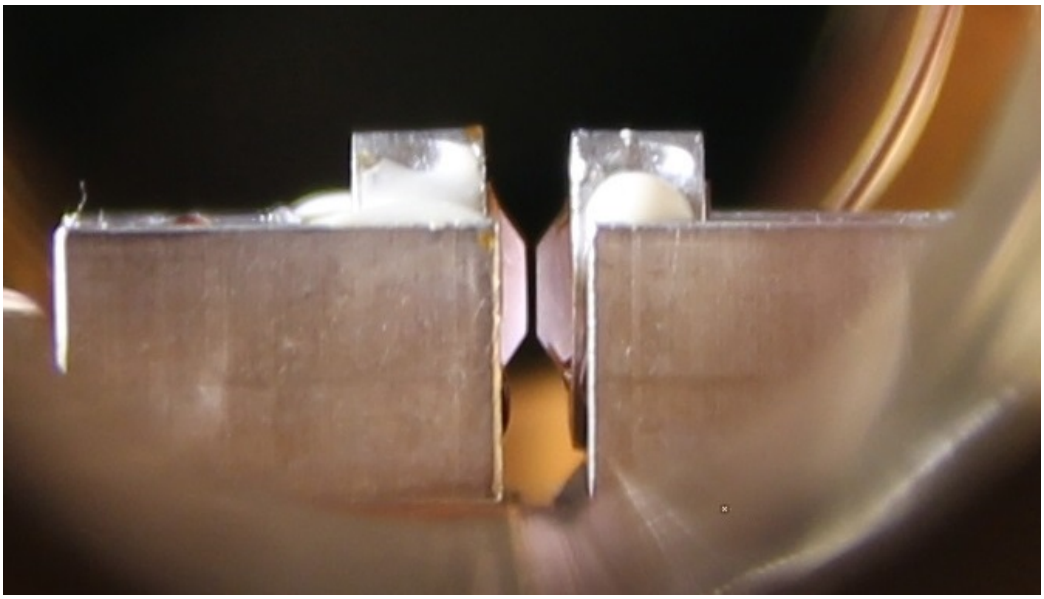

Figure 3.5: Picture of cavity within the vacuum chamber taken from a side angle viewport.

3.4 Self-feedback setup

The self-feedback component of the setup was entirely new and was the first time we attempted to apply any sort of feedback mechanism to a cavity QED system. We had the choice of a few ways of implementing this feedback; we could take the light from either the input or output mirror and also feedback it back into either mirror as well. Due to ease of setup, it was decided to apply feedback by collecting the reflected signal at the input mirror of the cavity and feedback it back into the same mirror with a controllable phase shift. The setup is quite similar to the network scheme discussed in Section 2.2.2. If you take the left configuration in Figure 2.9 but send the feedback beam back into the same port you collected it from, you get the topology we implemented in the lab. Schematically, the method of feedback implementation is shown in Figure 2.12.

For successful implementation of self-feedback in this setup, we need to achieve two things. Firstly, we need to define a reflection path which allows the reflected probe beam from the cavity to be routed to an area where it can be manipulated and put back into the input cavity mode. Secondly, that path that the reflected probe traverses needs to be stabilized by a different axillary beam which does not interfere in any way with the delicate feedback mechanism.

3.4.1 Feedback path and control

Finding an optimal way to apply the feedback was a bit challenging. As discussed earlier in Section 3.3, we have a cavity which experiences an appreciable amount of birefringence. Due to this, we cannot use circular polarized light and the polarization optics tricks that allow for the easy separation of co-linear beams. Stuck with the use of linearly polarized light, we had to be more creative with the feedback scheme and the use of a beamsplitter at the input in Figure 2.12 now probably makes more sense. Figure 3.6 shows an overhead shot of the input optics table with the input probe beam and feedback overlaid on top.

The first component the probe beam interacts with is a beamsplitter, though it is not your ordinary beamsplitter. A dichroic beamsplitter (Semrock LPD01-830) is used (it will become more apparent later on as to why) to provide a 80:20 power split of our 852nm probe by adjusting the angle of incidence. Right off the bat we throw away 80% of our probe beam. Since most of our experiment will occur with very weak probes, we are not starving for power and can afford to do this. However, now on the reflected signal, we can capture 80% of the light for our feedback scheme. You

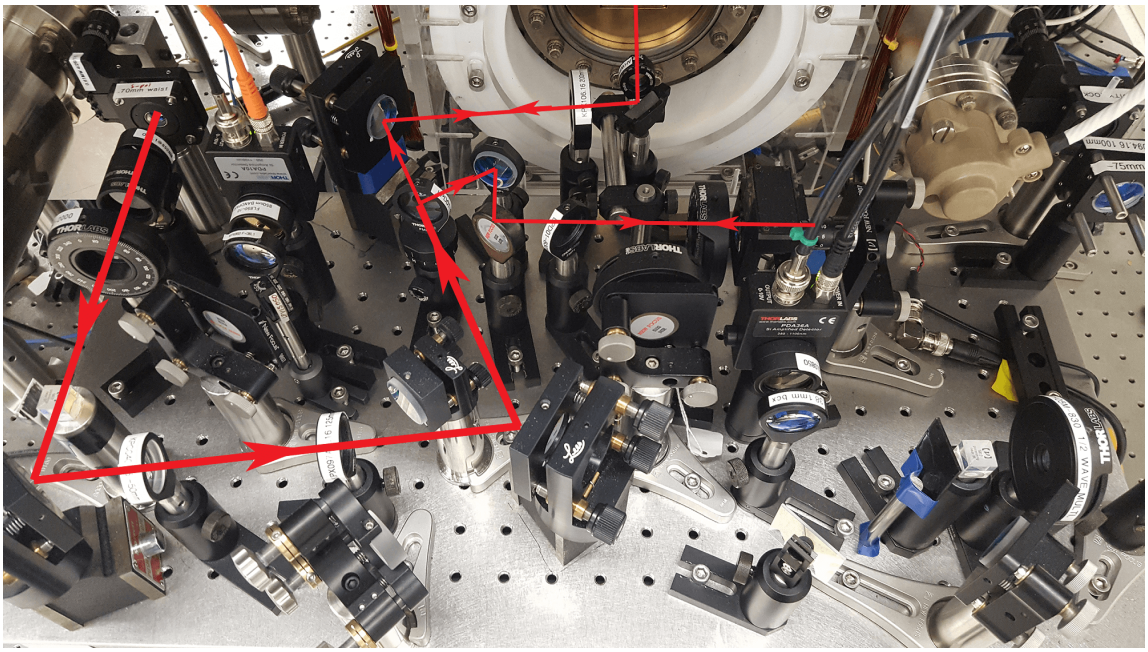

Figure 3.6: Overhead view of the input optical table showing an overlay of how the optical probe beam traverse the feedback path.

may wonder why I did not push that value up more to capture as much feedback light as possible? If you think about it, the way the feedback path is to be implemented you can form an external cavity with the input mirror of the science cavity and bottom mirror of the feedback path. Having a lossy beamsplitter allows us to avoid this while still providing enough feedback light to achieve the desired results.

The beam then propagates through the standard set of lenses and waveplates, gets reflected back on itself and comes back to the beamsplitter. Now we pick off 80% of the reflected signal to be processed in our feedback path. Within the feedback path, the beam is first passed through another dichroic beamsplitter (Semrock LPD01-830) but at an angle such that practically 100% of the 852nm probe light gets transmitted. The purpose of this dichroic is to filter out any of the locking

825nm beam from the feedback path. The beam then travels through a liquid crystal variable waveplate (Thorlabs LCC1113-B). This is a pretty neat little optic, allowing the control of the optical birefringence between the two axis by varying the amplitude of a AC square wave. Having such a control will prove very useful for our experiment. Lastly, the beam travels through a lens and gets focused down to a small mirror which is mounted on a piezo stack. This piezoelectric actuator will give us the ability to lock the overall feedback phase to any arbitrary phase of our choosing. The beam is reflected from this mirror and travels back through the described beam path into the cavity mode.

3.4.2 Feedback pathlength lock

In order to stabilize the beam path discussed above, we must use a separate locking beam which is off resonance to all the frequencies of interest and also the opposite polarization compared to the probe beam. To generate such a beam, we utilize one of our homemade external cavity diode lasers. This diode laser is frequency stabilization to the repumping $F = 3 \rightarrow F' = 4$ D_2 transition using a cesium saturated absorption setup. Since we will be needing to cancel out the DC component of the interference fringe of this beam interfering with itself, the intensity of the beam must not drift as it travels through various fiber lines to the input optics table. We utilize an intensity servo that uses an acousto-optic modulator before the final fiber to stabilize the beam intensity at the point of interest (component 1 in Figure 3.7). This lock beaming is injected into the input optics table via the same fiber EOM as the science cavity locking beam. This path is set up to be S-polarized light which is combined with the P-polarized probe beam on a polarizing beamsplitter (component 2 in Figure 3.7).

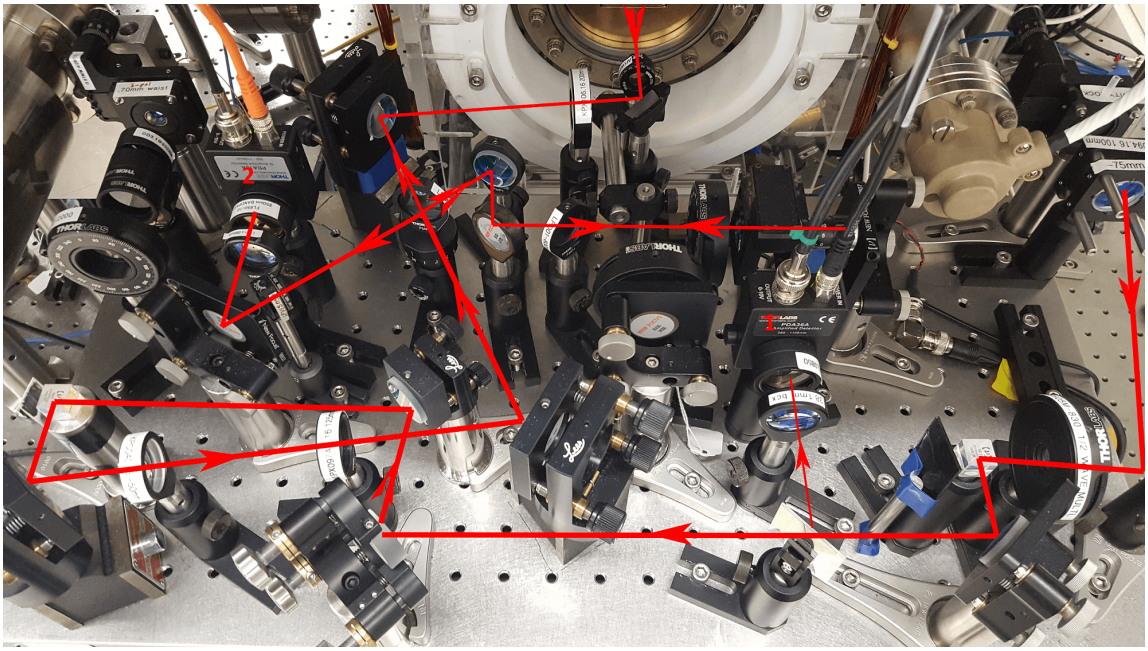

Figure 3.7: Overhead view of the input optical table showing an overlay of how the locking beam traverse the feedback path. Component 1 is the photodetector used for the intensity servo. Component 2 is the photodetector where the error signal is generated for the pathlength lock.

Now that the locking beam is co-linear with the probe beam, we will see how it traverses the optics along the way. The first dichroic beamsplitter sends a portion of the locking beam to a photodetector which will be used to monitor the interference pattern when we self interfere the locking beam onto itself. The portion of the locking beam which transmits through the dichroic will traverse the exact same path length which the probe beam travels. On its third time at the dichroic beamsplitter, the transmitted portion is sent to the same photodetector we referred to earlier. At this photodetector we have two beams interfering with each other where their pathlength difference is exactly the feedback path we are attempting to lock. You will notice that just before the detector there is a linear polarizer. Its purpose is to filter out any

of the probe beam which makes it to this area since it will impart large DC signals on the photodetector. Now there is a very large DC component to this signal from the interference and we must zero that out using the servo electronics before we can move forward. What remains is a very small fringe signal which oscillates with the pathlength fluctuations of our feedback path. Using a standard PI servo controller, we use the fringe signal from the photodetector as our error signal and lock this pathlength by feeding back to the piezo on the tiny mirror at the end of the feedback path.

You may be wondering how all these components come together to provide us with the locking and control we require. Our pathlength of interest is now locked such that the two portions of the locking beam are 90° out of phase. But for our experiment we really don't care about the phase difference of the locking beam, we are concerned only about the phase difference of our probe beam. This is where the liquid crystal variable waveplate comes into play. Remember that our probe beam and locking beam are two orthogonal polarizations. We set up our variable waveplate such that the slow and fast axis of the waveplate aligns with the s and p polarizations of the light. Now as we adjust the birefringence via the electronic control, the relative phase difference on the locking beam will remain at 90° since this change is slow enough for the servo to always maintain its lock. However we are continuously changing the relative phase difference between the two polarizations and therefore giving us full range of continuous tuning of the phase in the feedback path for the probe beam. In practice, the servo lock is very finicky and much care must be taken not to disturb the optical table.

When performing experiments, we did not map our electronic control of the feedback phase to the absolute phase. We were however able to easily set the system to a few fixed phase points. If we measure the output of the cavity with feedback in place, the output power will oscillate in correlation with the pathlength fluctuations of the feedback. To lock the feedback phase of the probe beam to $\phi_{fb} = 0$, we vary our control knob until we maximize the measured output. In this condition, the first incident probe beam and the reflected feedback probe beam constructively interfere, in essence increasing the effective drive of the cavity. Conversely, to lock the feedback phase of the probe beam to $\phi_{fb} = \pi$, we vary our control knob until we minimize the measured output. In this condition, the first incident probe beam and the reflected feedback probe beam destructively interfere, in essence decreasing the effective drive of the cavity.

3.5 Heterodyne measurement setup

The measurement setup for our experiment is very important to the quality of our measurements and thus we will spend some time going over the basics. From the cavity, the output light is routed to a 50:50 beamsplitter element where it is combined with the local oscillator beam. Each of the two output ports of the beamsplitter now have parts of both beams co-linear. These combined beams are put onto a high speed photodetector where they are detected. This interferometric method of detection is quite powerful, allowing us to measure extremely weak optical signals since the measurement is shot noise limited (or near). Figure 3.8

Let's work out some simple expressions for out detected signals. The operators for

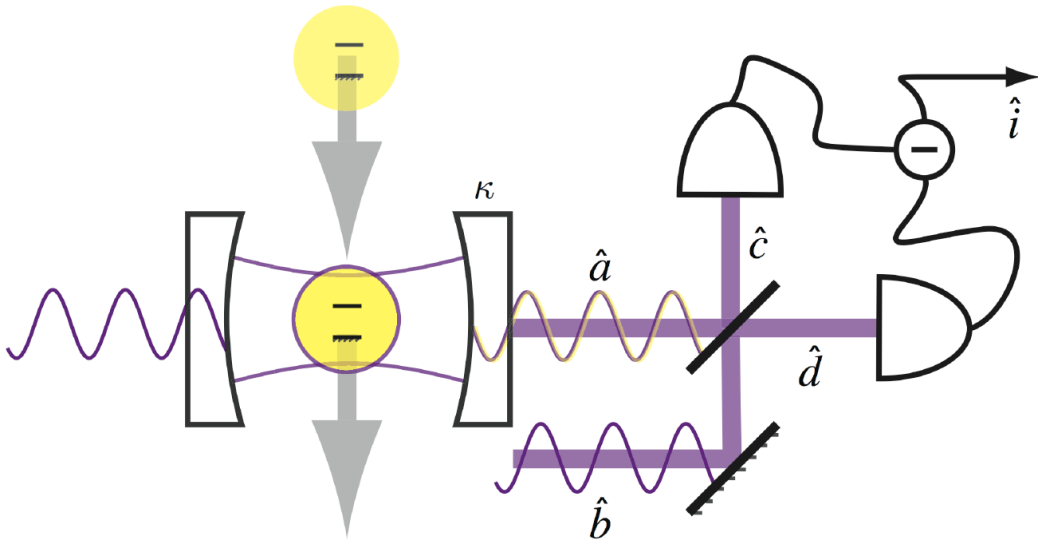

Figure 3.8: Schematic of the interferometric homodyne/heterodyne detection system.

the two fields incident on the photodetectors

$$\hat{c} = \frac{\hat{a} + \hat{b}}{\sqrt{2}} \tag{3.8}$$

$$\hat{d} = \frac{\hat{a} - \hat{b}}{\sqrt{2}} \tag{3.9}$$

where $\hat{a}$ is the output field from the cavity $\hat{b}$ is the local oscillator beam. The combined signals are then subtracted in the balanced photodetector to product an output signal

$$\begin{aligned} \hat{i} &= \hat{c}^\dagger \hat{c} - \hat{d}^\dagger \hat{d} \\ &= \hat{a}^\dagger \hat{b} + \hat{b}^\dagger \hat{a} \end{aligned} \tag{3.10}$$

If we substitute for the local oscillator the expression for a coherent state such that $\hat{b} = |\beta| e^{i\theta}$, we get

$$\hat{i} = |\beta|(e^{i\theta}\hat{a}^{\dagger} + e^{-i\theta}\hat{a}) \tag{3.11}$$

The large amplitude of the local oscillator acts as a gain term, allowing us to overcome all electronic noise with the measurement setup and only be limited by intrinsic sources. Now, for the heterodyne measurement, the local oscillator is slightly detuned from the signal we are measuring. This causes an interference fringe at the output of the balanced detector which oscillates at the detuning frequency. We can use the oscillating feature to sweep the entire phase space, in turn measuring two orthogonal quadratures of the output field quasi-simultaneously. Our in lab measurement setup is shown in Figure 3.9. We take out the output of the balanced detector and send it through a 0° RF splitter. Each of those two outputs are then mixed down using a RF mixer where the local oscillator signal is a RF signal at the heterodyne detuning frequency. By having the two LO signals differ by 90° in phase, we are able to measure two orthogonal quadratures.

If we apply a sine and cosine transform to Equation 3.11, we get

$$\begin{aligned}\hat{i} &= |\beta|(e^{i\theta}\hat{a}^{\dagger} + e^{-i\theta}\hat{a})\frac{(e^{i\omega_H t} + e^{-i\omega_H t})}{2} \\ &= \frac{|\beta|}{2}(e^{i2\omega_H t}\hat{a}^{\dagger} + e^{-i2\omega_H t}\hat{a} + \hat{a}^{\dagger} + \hat{a})\end{aligned} \tag{3.12}$$

$$\begin{aligned}\hat{i} &= |\beta|(e^{i\theta}\hat{a}^{\dagger} + e^{-i\theta}\hat{a})\frac{(e^{i\omega_H t} - e^{-i\omega_H t})}{2i} \\ &= \frac{|\beta|}{2i}(e^{i2\omega_H t}\hat{a}^{\dagger} - e^{-i2\omega_H t}\hat{a} - \hat{a}^{\dagger} + \hat{a})\end{aligned} \tag{3.13}$$

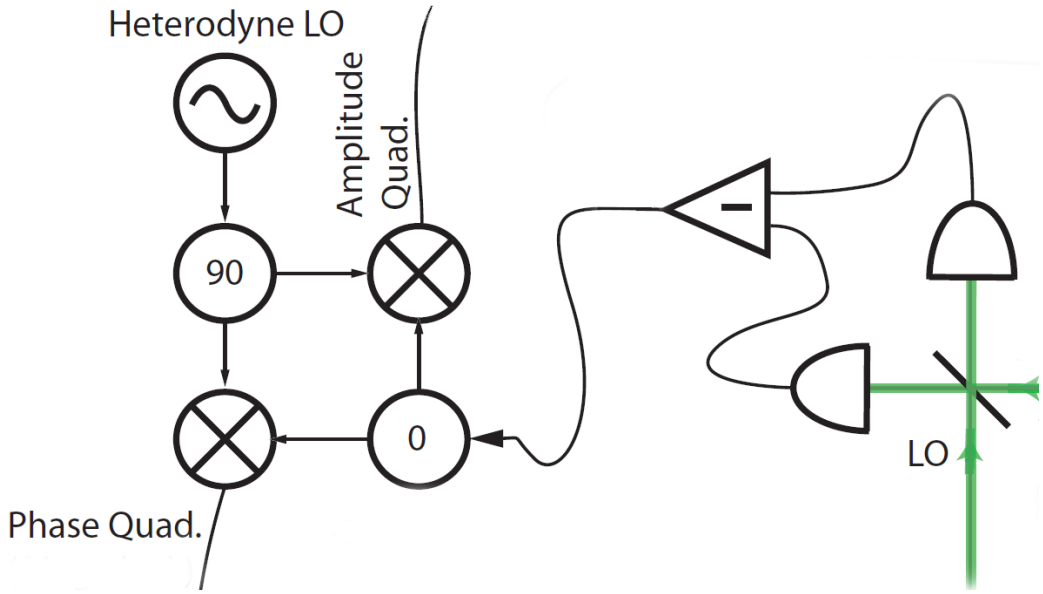

Figure 3.9: Schematic of the interferometric homodyne/heterodyne detection system.

Low pass filtering both of these signals we obtain the two quadratures

$$\begin{aligned} \hat{x} &= \frac{|\beta|}{2}(\hat{a}^\dagger + \hat{a}) \\ \hat{y} &= \frac{i|\beta|}{2}(\hat{a}^\dagger - \hat{a}) \end{aligned} \tag{3.14}$$

3.5.1 Calibration of output measurements

In order to analyze the signal we measured, we first must have calibrated output measurement schemes that allow us to work out to high accuracy the power of the output beam. For quick diagnostics, we have a Hamamatsu APD available at the flip of a mirror. It can be used down to nW power levels. In order to calibrate its response, we compared the measured output voltage to the power measured from a calibrated Thorlabs power meter. Since the response of the APD is highly linear, we can expect that responsively measurements made at higher optical power levels will

still hold true at lower levels. With the noise floor zeroed out, the APD responds such that

$$V_{APD} = 5 \times 10^8 \cdot P_s \tag{3.15}$$

where V_{APD} is the output voltage measured from the APD detector and P_s is the optical power of the signal of interest.

We also have to characterize the response of the total heterodyne detection setup. That first begins by determining the responsivity of the balanced detector. By knowing the incident power levels of both the signal and LO beams as well as their overlap efficiency, we should be able to extract the response. The overlap efficiency, or homodyne efficiency η_H, is a metric of how well the modes of the optical output signal and LO overlap at the photodetector. To calculate it, we interfere in one arm of the heterodyne setup equal power signal and LO beams. This gives us a DC signal with a AC wiggle from the time varying relative phase. Since the measured voltage from the photodetector is proportional to η_H, by just measuring the max and min of the interference signal, we get

$$\eta_H = \frac{I_{max} - I_{min}}{I_{max} + I_{min}} \tag{3.16}$$

Doing this for our setup, we find that the homodyne efficiency is ≈ 0.8. This is quite good. It took a lot of effort to get the efficiency this high. Since the output optics table is very cramped and in an awkward place, it was hard to really get in there to manipulate the optics to maximize this. I used a beam profiling camera to ensure that the LO beam and the cavity output signal beam matched as well as possible

over the entire distance of the interferometer.

Now with the homodyne efficiency η_H in hand, we can measure the responsivity of the balanced detector. By looking at the peak-to-peak voltages of the AC signals produced, it was calculated that the responsivity $\mathcal{C} = 3.2 \times 10^4\, V/W$.

We take out heterodyne signal, which in our experiment has a frequency detuning of $25MHz$, and put it through RF electronics to mix it with a sine and cosine LO signals. The output of the RF mixers are low pass filtered at $5MHz$. By measuring all the input-output relations of the signals as they propagate through the RF circuitry, we can get an overall expression which relates the output optical signal to the measured amplitude quadrature heterodyne with 50Ω input coupling

$$V_{H,50\Omega} = 2.769 \times 10^3 \cdot \sqrt{P_s} \tag{3.17}$$

Chapter 4

Measurements and Results

4.1 Cavity parameter control with coherent feedback

With our self-feedback configuration in place and electronics setup to lock the system and give us control, we are able to begin measurements system dynamics and how they are affected by the feedback. Like we predicted in Section 2.2.3, the output power oscillated around the nominal output with the application of feedback. We used measure to set the feedback phase to the two extreme cases in order to perform the experiments.

The first and easiest thing to measure is the cavity linewidth. If you remember from Figure 2.14, the cavity linewidth strongly depends on the feedback phase of the network. The overall linewidth can be either greater or smaller than the nominal no feedback linewidth. Like previously discussed, depending on if the feedback signal is constructively or destructively interfering with the probe beam, the input mirror's

effective transmission is altered. This is also what gives rise to the phase dependant effective drive.

In order to measure the linewidth, cavity ringdown measurements were performed on the system. Since the probe beam generated as a sideband by the fiber EOM it travels through, we had the ability to rapidly modulate the probe on and off using an RF switch. This RF switch was driven by a square wave driven at $10kHz$, allowing enough time for the cavity intensity to build up and also dissipate. Due to the microscopic size of the cavity, the cavity relaxation time is on the order of $100ns$ even though the finesse is very high. In order to actually measure this accurately, we used a high speed photodetector on the output. By looking at the output with a modulated input beam, we can fit an exponential decay to the cavity response once the input is turned off, thus giving us a measure of the linewidth. This measurement was done in three instances: with no feedback, with feedback and $\phi_{fb} = 0$, and with feedback and $\phi_{fb} = \pi$. Table 4.1 shows our measured results.

The measured linewidth of the cavity in the no feedback configuration was not quite as narrow as the theoretical value of $\delta f = 1.6MHz$. Using our measured linewidth value, we have a measured finesse $\mathcal{F} = 222,000$. As we talked about previously, the quality of the cavity degrades as it is exposed to ambient cesium gas in the vacuum chamber.

Feedback Phase ϕ_{fb}	**Cavity Linewidth (MHz)**
No feedback	2.25 ± 0.08
0	2.86 ± 0.09
π	1.83 ± 0.20

Table 4.1: Cavity linewidth at various feedback phase settings

We were able to directly control the linewidth of our cavity QED system over a large range with the application of feedback. Having such a knob in experiments can be quite useful as it allows you to explore various parameter regimes of cavity QED without having to alter the mechanical design of the cavity.

4.2 Atom cloud dynamics

We have talked about how we generate and control the atom cloud previously in Section 3.2. However since our method of delivering the atoms is to drop them and let them fall under the influence of gravity through the narrow cavity, we can get wildly different results drop to drop.

4.2.1 Using transmission data to back infer atom cloud distribution

How can we go about determining the number of atoms with the cavity mode at some time and also their distribution? Let's go back to the semi-classical description for a multi-atom system and take a closer look at the equation. In the situation of no detuning, Equation 2.1.2.1 reduces to

$$|y| = |x_{ss}| \left(1 + \sum_{j=1}^{N} \frac{2c_j^2 C_0}{1 + c_j^2 |x_{ss}|^2} \right) \tag{4.1}$$

Now let's assume we are in a regime well above the nonlinear response such that the atoms are mostly saturated. The term in the denominator can thus be simplified as follows

$$
\begin{aligned}
|y| &\approx |x_{ss}| \left(1 + \sum_{j=1}^{N} \frac{2c_j^2 C_0}{c_j^2 |x_{ss}|^2}\right) \\
&\approx |x_{ss}| \left(1 + \frac{2C_0}{|x_{ss}|^2} \sum_{j=1}^{N} \frac{\cancel{c_j^2}}{\cancel{c_j^2}}\right) \\
&\approx |x_{ss}| \left(1 + \frac{2C_0 N}{|x_{ss}|^2}\right)
\end{aligned}
\tag{4.2}
$$

Visually, we are working in a regime where the response is only a small dip from the empty cavity response, as shown in Figure 4.1.

Ok, let's take our new approximation and try to back calculate the number of atoms using transmission data. Just note that the MBE description is approximate and in certain situations does not match the actual result. This method is just to give us an approximation as a starting point. Figure 4.2 is a capture amplitude quadrature heterodyne signal which shows a dip in the transmitted signal due to the cloud passing through the cavity mode. This dip is quite small since we are far away from the nonlinear response region.

Using the approximation is Equation 4.2, we back calculate the atom number corresponding to this response. Figure 4.3 gives us that result. What we get is that we are in regime where there are only a handful of atoms entering the cavity mode at a time or effectively contributing to the response. This 15-20 atom regime is perfect if we want to study the so called mesoscopic regime.

As a check, we can do a Monte Carlo simulation of an atom cloud thermally

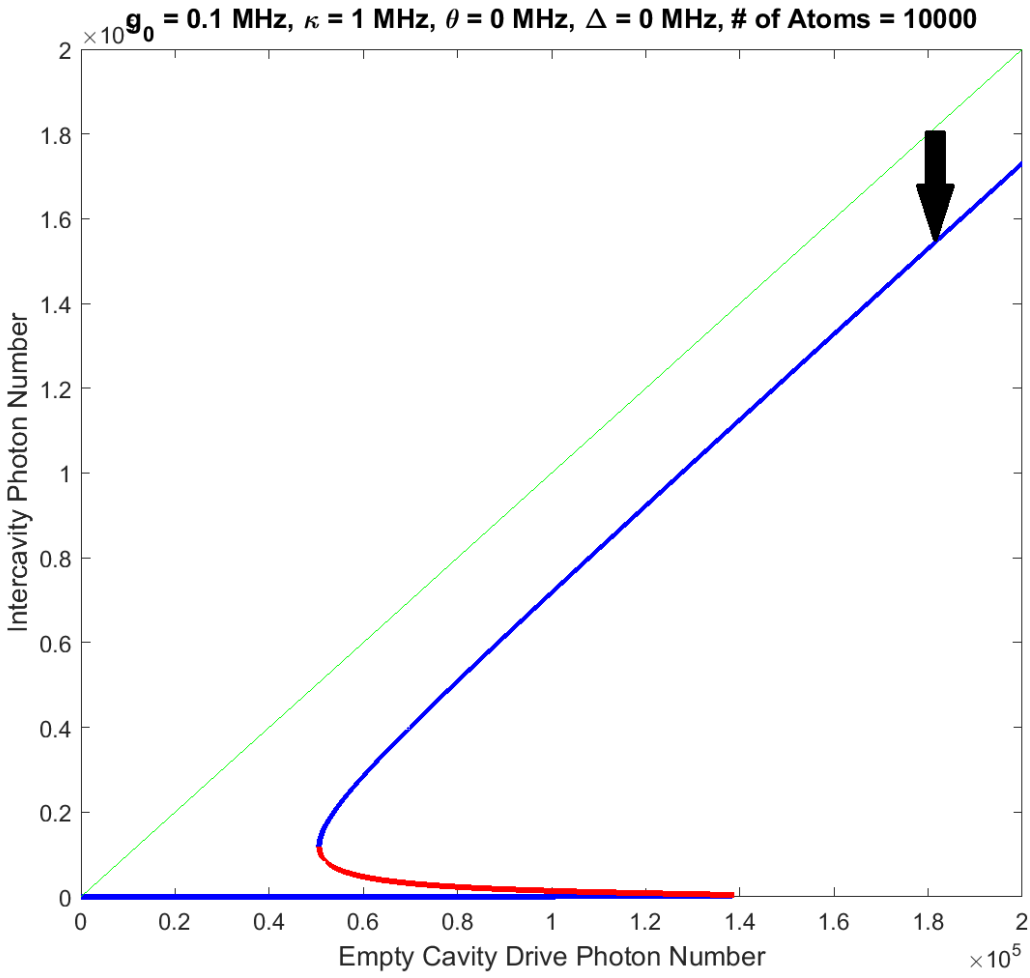

Figure 4.1: Amplitude quadrature heterodyne signal with constant probe as atom cloud drops through cavity mode. The red curve depicts the empty cavity response and the blue curve is the measured heterodyne signal.

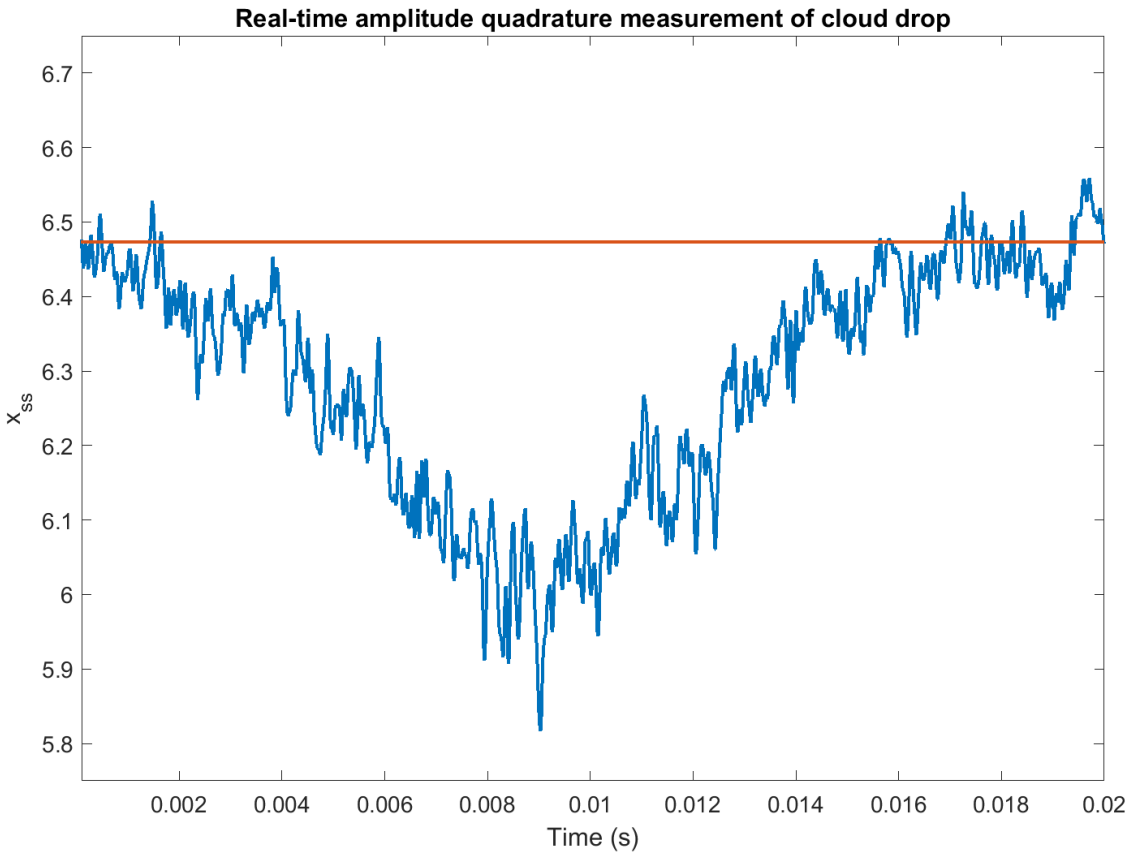

Figure 4.2: Amplitude quadrature heterodyne signal with constant probe as atom cloud drops through cavity mode. The red curve depicts the empty cavity response and the blue curve is the measured heterodyne signal.

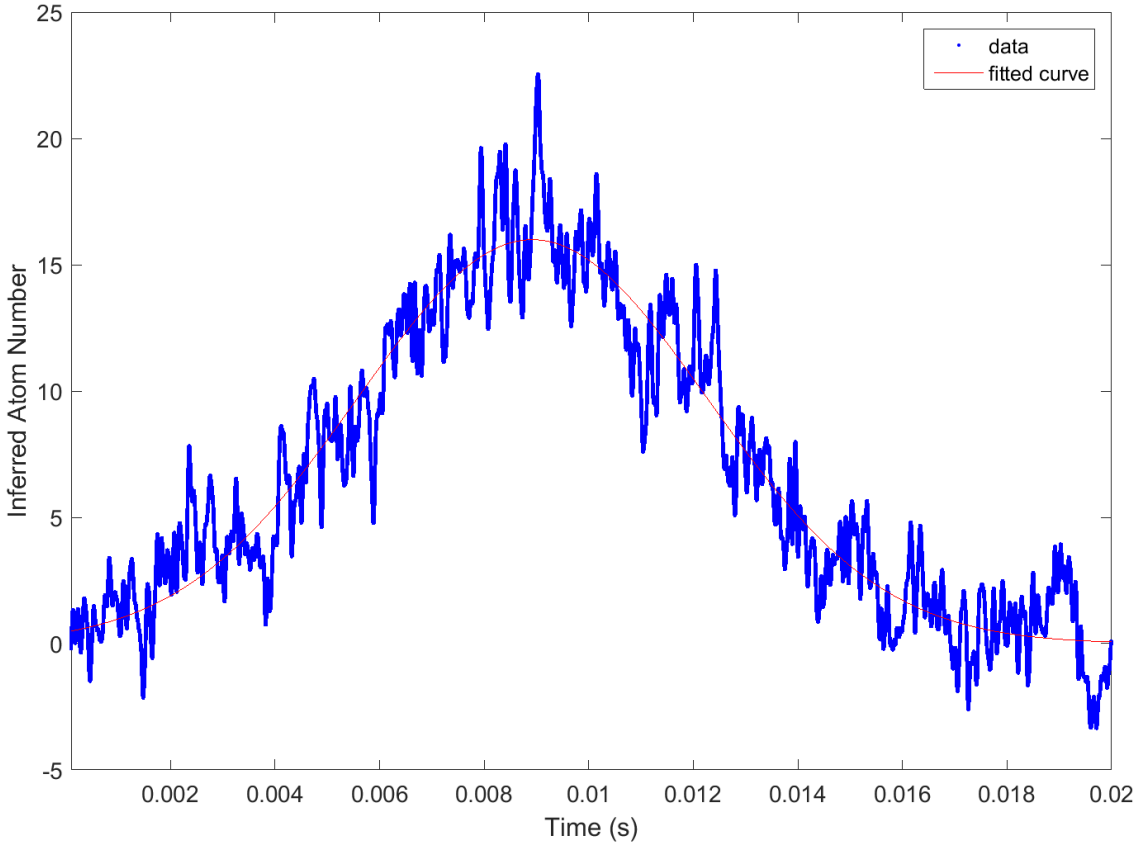

Figure 4.3: Inferred atom number over time as cloud drops through cavity mode.

expanding and falling under gravity. We set up a simulation where we have a cloud of 5×10^5 atoms positioned $13mm$ above the cavity mode. The cloud is cooled to a temperature of $25\mu K$. The cavity parameters are the same as the ones used in the experiments. Figure 4.4 shows that even in simulations we get an approximate atom number in the range of 15-20 in the cavity mode. In the simulation we actually count the number of atoms within the cavity mode as we propagate them in time. What we count as *in* the cavity is any atom within two Gaussian waists of the cavity axis.

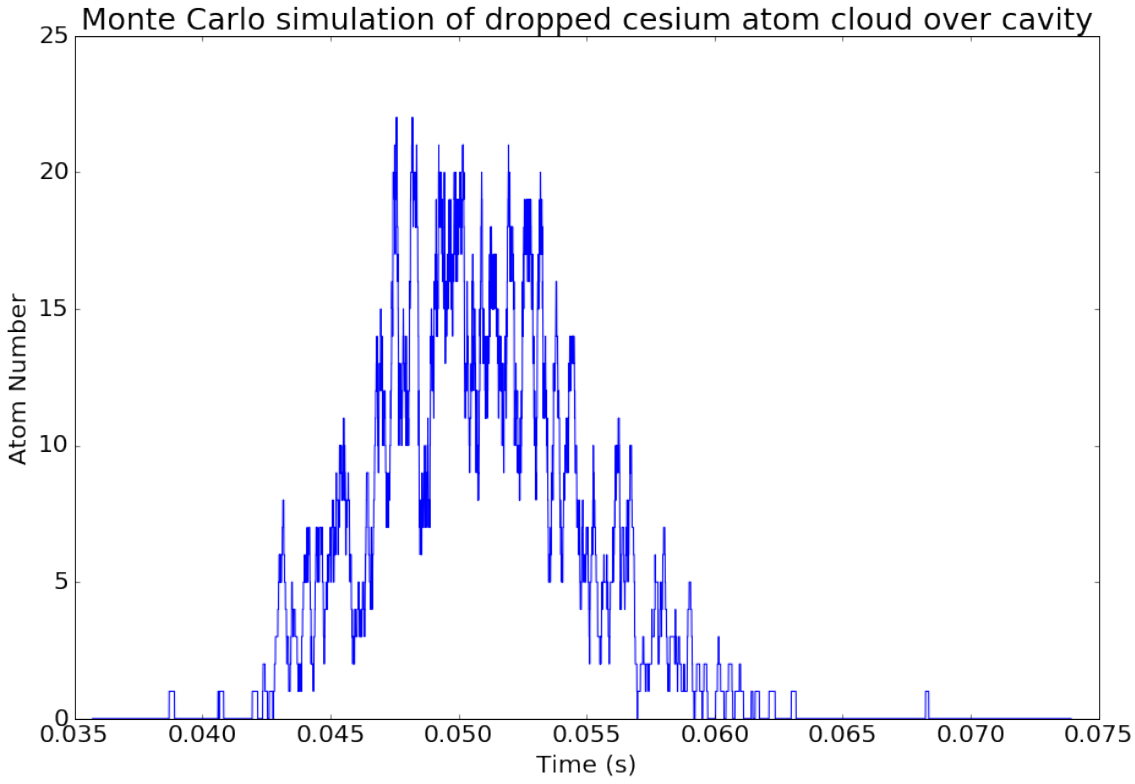

Figure 4.4: Simulated atom number within cavity mode as cloud falls.

4.3 Real time amplitude bistability

With our system, we looked at atom dynamics and approximate distribution within the cavity mode. Even though we cannot obtain the theoretical maximum atom-cavity coupling, due to the polarization of the input light but also the motion of atoms through the cavity mode, we still have a situation where the nonlinear response is strong enough to see interesting behavior in a regime of low energy probe.

To start, we find the lowest probe level needed to not have the atom interaction cause the cavity to *dark*. What I mean by that is that the nonlinearity is so strong that the intracavity cavity field in practically brought to zero. Find that minimum level, we now have a range of input amplitudes to sweep over such that we make sure the system can go through its entire hysteretic behavior. Since the time it takes an atom to traverse through the cavity mode is on the order of $\approx 100\mu s$, we need to make sure that we are sweeping our probe fast enough that we get a handful of periods of the response in that time. Since we are assuming that the atom is momentarily stationary within the while we are probing, our sweep is required to be fast. Therefore, we decide to with a sweeping frequency of $100kHz$. This gives us about 10 periods while the atom travels through the cavity mode. We use a RF in reverse to impart the $100kHz$ modulation on top of the RF signal that drives the EOM that generates the probe beam. The shape of the modulate is sawtooth, giving us linear sweep of the cavity input field.

With one quadrature of the heterodyne measurement locked to zero, the other signal provides us with the measure of the amplitude quadrature. This signal is recorded via the DAQ at a rate of $200MHz$ over a large $20\mu s$ window, with the atom

drop approximately located in the middle of that time window. A large acquisition window gives enough wiggle room to make sure we capture everything.

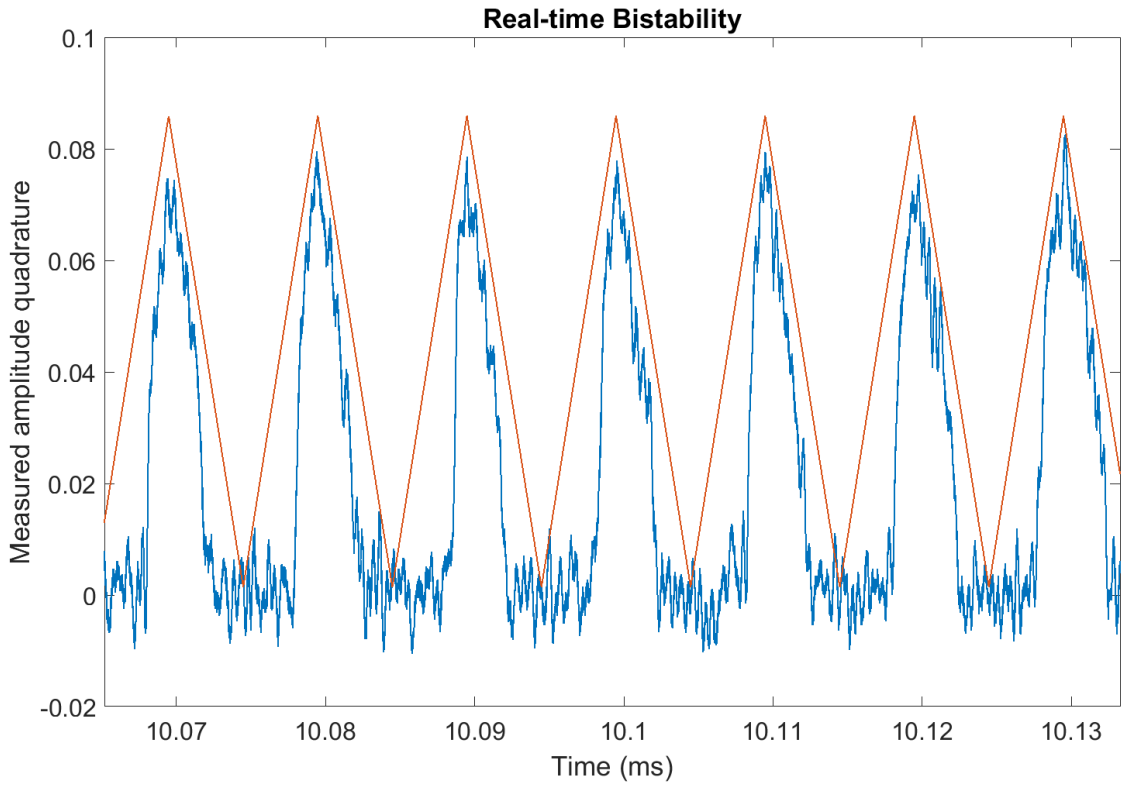

Figure 4.5: Captured amplitude quadrature signal showing the output of cavity QED experiencing real-time bistability. The red curve is a guide that shows the empty cavity response and also the input drive field. The blue curve is the output field which atoms are present in the cavity.

The raw output signal, as shown in Figure 4.5, shows very clear signs of hysteretic behavior. As we are sweeping our probe from low to high, you can see the intracavity field being suppressed to a point where it suddenly jumps to a high level. Going in reverse, the cavity field follows the input, with the nominal loss due to absorption,

to a point where it suddenly falls to a low state. The drive levels where these sudden jumps occur are not equal, as can be seen by the asymmetrical shape of the curves.

Let's now take this data and try to plot input/output behavior of this system. First it is key to find a region in the captured dataset where strong nonlinear response occurs and where that response is fairly constant over a few periods. Since the atom delivery mechanism is so sporadic, it can be difficult to find *good* datasets. The first set of experiments are done with no feedback in place. We take the raw data and find the best few sweeps. Plotting the input/output behavior of the system in this region, we get the response as shown in Figure 4.6. The red curves are for sweeps from 0 drive to the maximum and conversely the blue curves are for sweeps from high drive to 0. The light shaded curves are the actual data traces from the real-time bistability. For this plot, we took six consecutive periods and plotted them on one plot. The dark red and blue traces are the averages of those six up/down sweeps. The bistability is clear and prominent in this system. Pay attention to the input drive values that this behavior is occurring at.

Next, we used our self-feedback scheme to control the cavity QED parameters to see if it has affects on the dynamics of the system. We set the feedback phase such that $\phi_{fb} = 0$. Again we sweep over a range such that we fully go through the hysteretic region. Figure 4.7 shows the input/output behavior of this system. This time, we were only able to find three consecutive periods to plot. Once again, the bistability is prominent however it now is occurring at a lower input drive field in comparison to the no feedback case.

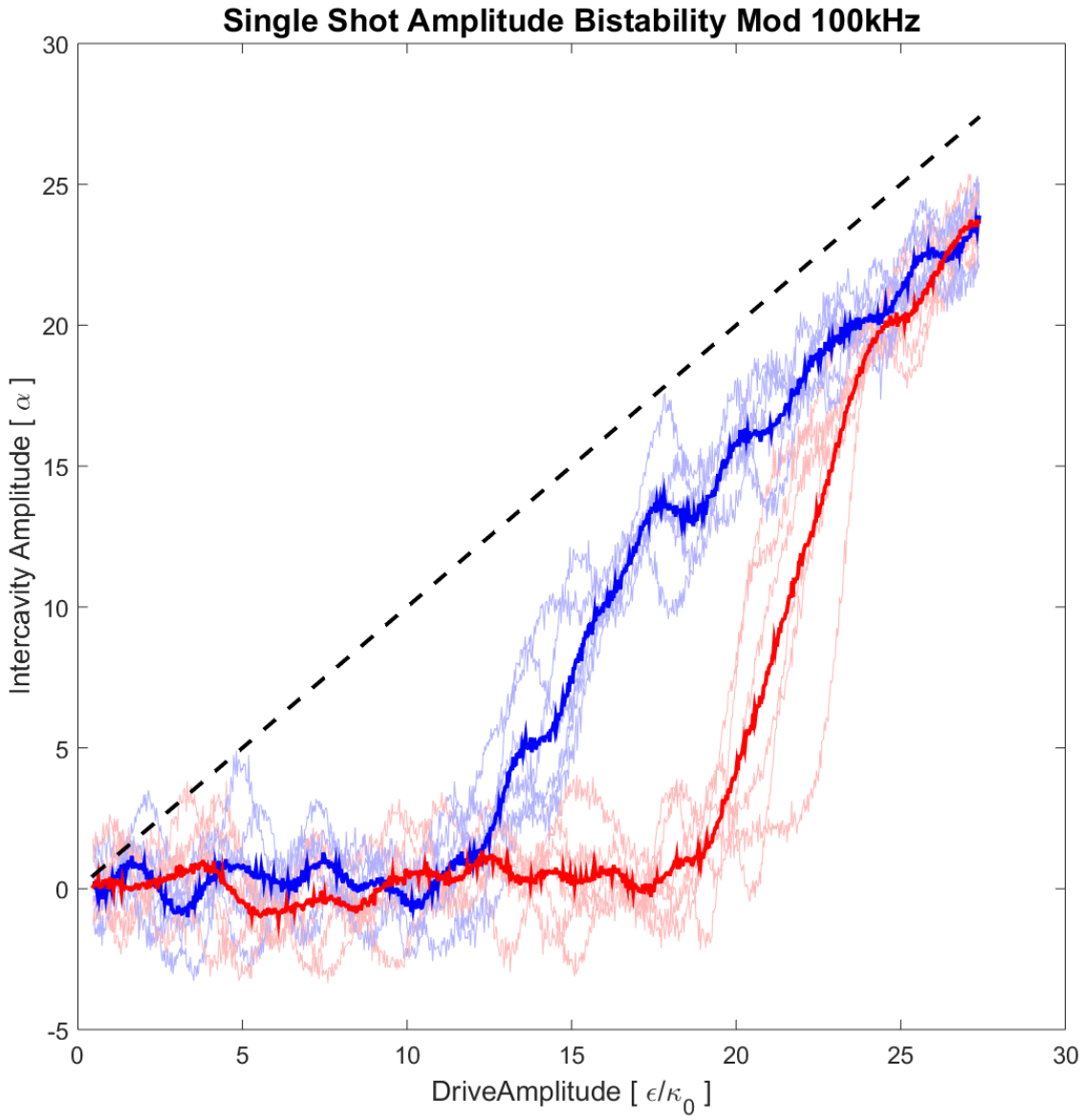

Figure 4.6: Real-time input/output relation of cavity QED system experience bistable response with no feedback.

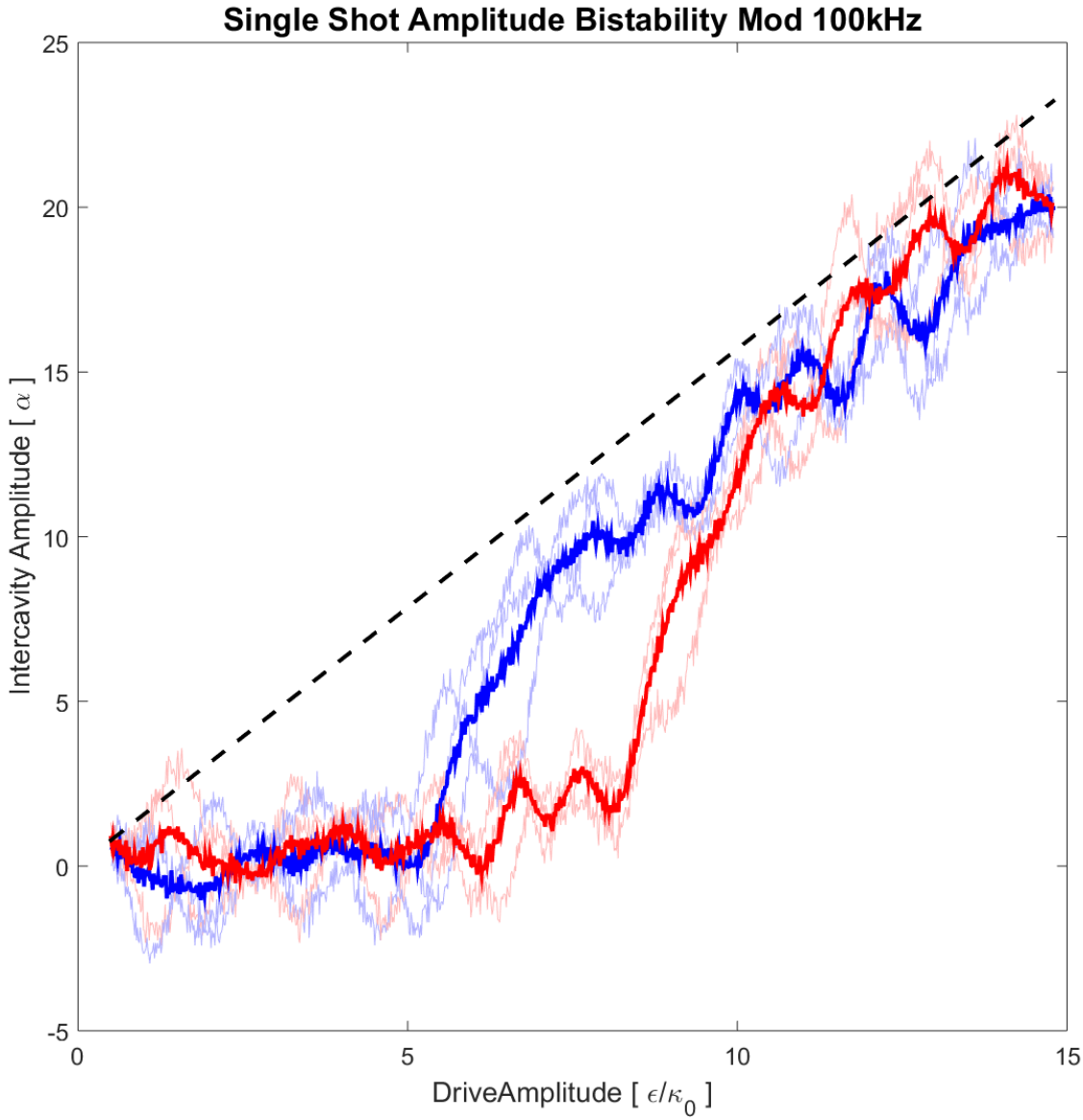

Figure 4.7: Real-time input/output relation of cavity QED system experience bistable response with feedback $\phi_{fb} = 0$.

Lastly, we set the feedback phase such that $\phi_{fb} = \pi$. Again we sweep over a range such that we fully go through the hysteretic region. Figure 4.8 shows the input/output behavior of this system. This time, we were able to find four consecutive periods to plot. Once again, the bistability is prominent however it now is occurring at a higher input drive field in comparison to the no feedback case.

In the three cases, we were able to collect very good data depicting real-time amplitude bistability. Such data is difficult to collect in this energy regime and thus is not a commonly done experiment. The feedback definitely has significant effects on the dynamics of the system by shifting the bistability region along the input drive axis and also affecting the width of the hysteretic response.

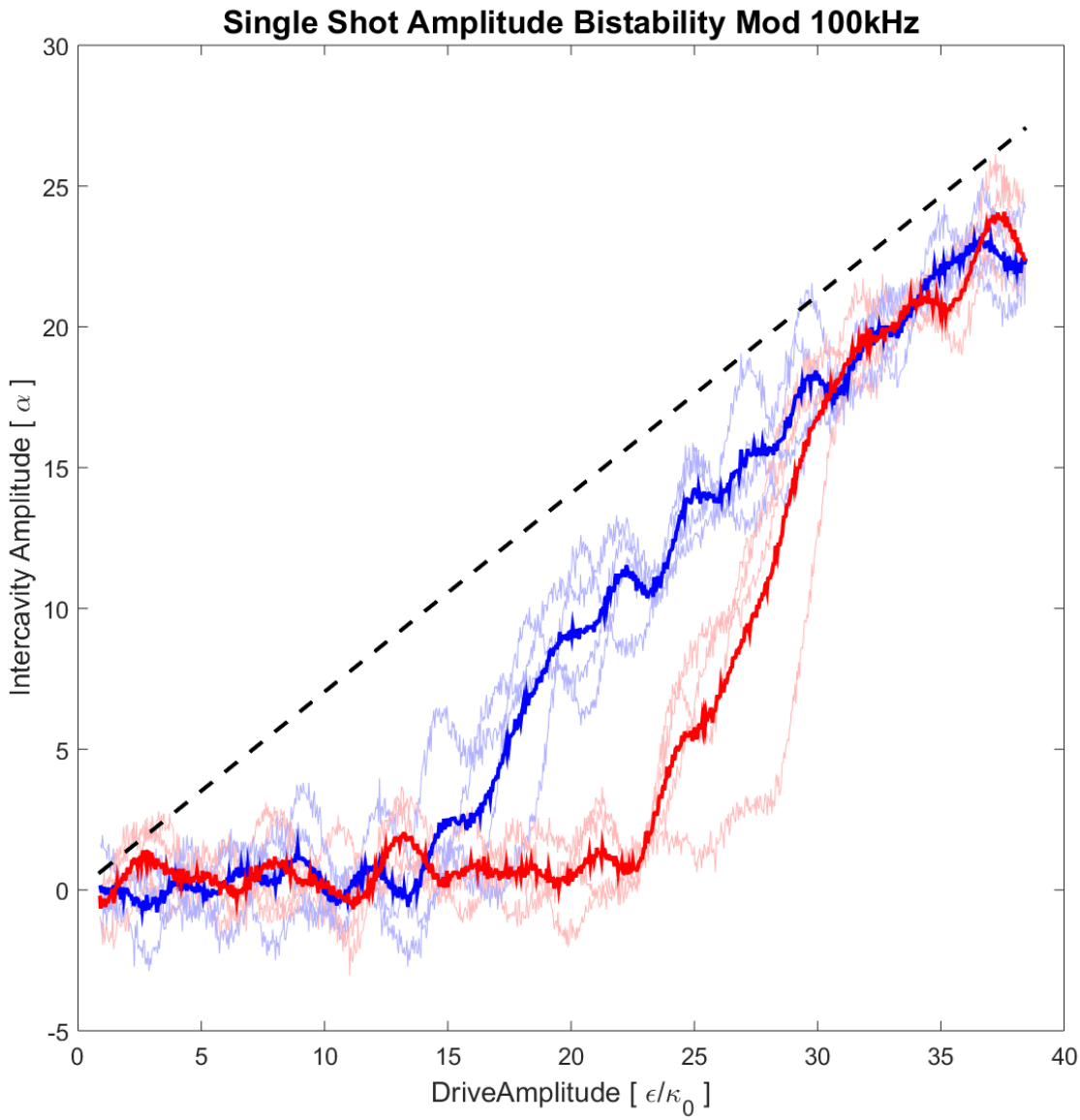

Figure 4.8: Real-time input/output relation of cavity QED system experience bistable response with feedback $\phi_{fb} = \pi$.

Chapter 5

Conclusions

Over the course of this thesis, we have explored the space of cavity quantum electrodynamics (QED). We have looked at specific examples of nonlinear behavior in these cavity QED systems and also the potential of forming quantum networks with such systems. These systems show nonlinear behavior which is quite intriguing from an information processing standpoint. We can observe simple switching mechanism in cavity QED based devices that occurs in the ultra low power regime. Tools and techniques exist to model such systems, allowing us to build complicated architectures of these photonic computing units.

The practical regime of interest to us lies somewhere between one that can be easily described and simulated quantum mechanically and one which can be fully explained using the simple semi-classical Maxwell-Bloch equations. This mesoscopic regime does not have a well developed theory and the jury is still out on how to approach such a parameter regime.

Additionally, we studied the case of a simple self-feedback network applied to a Fabry-Perot optical cavity. The use of coherent feedback gave us the ability to electronically control various cavity QED parameters of the system without having to physically alter anything. This is a powerful tool, opening up many possibilities and ways you approach such systems.

I did spend a majority of my grad school career in the lab building up and debugging the optical setup. Cavity QED systems are notorious for being extremely complicated and difficult to run. A large number of components must all work together at the same time in order to achieve experimental goals. At the end, I did however manage to collect interesting data from the system. Looking at absorptive bistability in the cavity QED system, we observed real time switching of the state in an energy regime low enough to be interesting. Also, by using the coherent feedback setup, we were able to see how these dynamics shift as you vary the experimental parameters.

There still lies a lot of work with respect to the modelling and theory for this project. The data set collected is a good starting point in the exploration of this space and gives us some intuition of what exactly is happening in these mesoscopic cases.

Bibliography

[1] H. J. Kimble. The quantum internet. *Nature*, 453(7198):1023–1030, 6 2008.

[2] Michael Riordan, Lillian Hoddeson, and Conyers Herring. The invention of the transistor. *Reviews of Modern Physics*, 71(2):S336–S345, 3 1999.

[3] Gordon E. Moore. Cramming more components onto integrated circuits, Reprinted from Electronics, volume 38, number 8, April 19, 1965, pp.114 ff. *IEEE Solid-State Circuits Newsletter*, 20(3):33–35, 9 2006.

[4] Robert W. Keyes. The Impact of Moore's Law. *IEEE Solid-State Circuits Newsletter*, 20(3):25–27, 9 2006.

[5] M. Mitchell Waldrop. The chips are down for Moore's law. *Nature*, 530(7589):144–147, 2 2016.

[6] John M. Shalf and Robert Leland. Computing beyond Moore's Law. *Computer*, 48(12):14–23, 12 2015.

[7] Ron Ho, Philip Amberg, Eric Chang, Pranay Koka, Jon Lexau, Guoliang Li, Frankie Y. Liu, Herb Schwetman, Ivan Shubin, Hiren D. Thacker, Xuezhe Zheng, John E. Cunningham, and Ashok V. Krishnamoorthy. Silicon Photonic Interconnects for Large-Scale Computer Systems. *IEEE Micro*, 33(1):68–78, 1 2013.

[8] Karl J. (Karl Johan) Astrom and Richard M. Murray. *Feedback systems : an introduction for scientists and engineers*. Princeton University Press, 2008.

[9] Howard Carmichael. *An Open Systems Approach to Quantum Optics*, volume 18 of *Lecture Notes in Physics Monographs*. Springer Berlin Heidelberg, Berlin, Heidelberg, 1993.

[10] Ryan Hamerly and Hideo Mabuchi. Advantages of Coherent Feedback for Cooling Quantum Oscillators.

[11] Hyatt M. Gibbs. *Optical bistability : controlling light with light*. Academic Press, 1985.

[12] H. Mabuchi, J. Ye, and H.J. Kimble. Full observation of single-atom dynamics in cavity QED. *Applied Physics B: Lasers and Optics*, 68(6):1095–1108, 6 1999.

[13] Joseph Kerckhoff, Michael A Armen, and Hideo Mabuchi. Remnants of semiclassical bistability in the few-photon regime of cavity QED. *Optics express*, 19(24):24468–82, 11 2011.

[14] Michael Armen. *Bifurcations in single atom cavity QED*. PhD thesis, 2009.

[15] Yeong-Dae Kwon, Michael A. Armen, and Hideo Mabuchi. Femtojoule-scale all-optical latching and modulation via cavity nonlinear optics. 5 2013.

[16] Paul E. Barclay, Kai-Mei Fu, Charles Santori, and Raymond G. Beausoleil. Hybrid photonic crystal cavity and waveguide for coupling to diamond NV-centers. *Optics Express*, 17(12):9588, 6 2009.

[17] H. Mabuchi and A. C. Doherty. Cavity Quantum Electrodynamics: Coherence in Context. *Science*, 298(5597), 2002.

[18] Joseph Kerckhoff, Michael A. Armen, Dmitri S. Pavlichin, and Hideo Mabuchi. The dressed atom as binary phase modulator: towards attojoule/edge optical phase-shift keying. *Optics Express*, 19(7):6478, 3 2011.

[19] Michael A. Armen, Anthony E. Miller, and Hideo Mabuchi. Spontaneous Dressed-State Polarization in the Strong Driving Regime of Cavity QED. *Physical Review Letters*, 103(17):173601, 10 2009.

[20] G. Rempe, R. J. Thompson, R. J. Brecha, W. D. Lee, and H. J. Kimble. Optical bistability and photon statistics in cavity quantum electrodynamics. *Physical Review Letters*, 67(13):1727–1730, 9 1991.

[21] J.R. Johansson, P.D. Nation, and Franco Nori. QuTiP: An open-source Python framework for the dynamics of open quantum systems. *Computer Physics Communications*, 183(8):1760–1772, 2012.

[22] Crispin W. Gardiner and Peter Zoller. *Quantum noise : a handbook of Markovian and non-Markovian quantum stochastic methods with applications to quantum optics*. Springer, 2004.

[23] J. Gough and M. R. James. Quantum Feedback Networks: Hamiltonian Formulation. *Communications in Mathematical Physics*, 287(3):1109–1132, 5 2009.

[24] J. Gough and M.R. James. The Series Product and Its Application to Quantum Feedforward and Feedback Networks. *IEEE Transactions on Automatic Control*, 54(11):2530–2544, 11 2009.

[25] Nikolas Tezak. *Scalable Techniques For Quantum Network Engineering*. PhD thesis, 2016.

[26] Nikolas Tezak, Armand Niederberger, Dmitri S Pavlichin, Gopal Sarma, and Hideo Mabuchi. Specification of photonic circuits using quantum hardware description language. *Phil. Trans. R. Soc. A*, 370:5270–5290, 2012.

[27] Hideo Mabuchi. Coherent-feedback control strategy to suppress spontaneous switching in ultralow power optical bistability. *Applied Physics Letters*, 98(19):193109, 5 2011.

[28] Hideo Mabuchi. Nonlinear interferometry approach to photonic sequential logic. *Applied Physics Letters*, 99(15):153103, 2011.

[29] Joseph Kerckhoff. *Quantum Engineering With Quantum Optics*. PhD thesis, 2011.

[30] R. W. P. Drever, J. L. Hall, F. V. Kowalski, J. Hough, G. M. Ford, A. J. Munley, and H. Ward. Laser phase and frequency stabilization using an optical resonator. *Applied Physics B Photophysics and Laser Chemistry*, 31(2):97–105, 6 1983.

[31] E. L. Raab, M. Prentiss, Alex Cable, Steven Chu, and D. E. Pritchard. Trapping of Neutral Sodium Atoms with Radiation Pressure. *Physical Review Letters*, 59(23):2631–2634, 12 1987.

[32] Harold J. Metcalf and Peter van der Straten. *Laser Cooling and Trapping*. Graduate Texts in Contemporary Physics. Springer New York, New York, NY, 1999.